

Abstract

LO, HUNGYING. Electromagnetic Field Calculation for a High-Frequency Wave in a Lossy Transmission Line. (Under the direction of Frank Kauffman)

The objective of this research is to calculate electromagnetic field distribution on the cross section of a lossy transmission line in a Multi-Chip Module(MCM) for predicting the performance of a high-frequency wave propagation in the module. Our approach is to use the hybrid edge/nodal Vector Finite Element Method (VFEM) and apply the 3-component Measured Equation of Invariance (MEI) boundary condition to the calculation. By using the hybrid edge/nodal VFEM the relation between propagation constant and the field distribution on the cross section of the transmission line is obtained, and by using 3-component MEI boundary the field distribution of an open transmission line is calculated with the limited computer resources. The propagation constant of a lossy transmission line with coated conductor strip is also calculated. This 3-component MEI boundary condition simulates the field propagation on the artificial boundary for the electromagnetic field excited from the surface charge, from the current distribution in the axial direction, and from the current distribution on the transverse plane of the transmission line. Numerical experiments are performed to test the numerical calculation with 3-component MEI boundary condition by comparing calculated transmission loss with the measured data. At high frequency, the calculated results are about 10% lower than the measured data. That's because the

ground loss is not included in the calculation.

**ELECTROMAGNETIC FIELD CALCULATION FOR A
HIGH-FREQUENCY WAVE IN A LOSSY
TRANSMISSION LINE**

by

HUNGYING LOUIS LO

A dissertation submitted to the Graduate Faculty of
North Carolina State University
in partial fulfillment of the
requirements for the Degree of
Doctor of Philosophy

DEPARTMENT OF ELECTRICAL ENGINEERING

Raleigh

1997

APPROVED BY:

Dr. J. W. Mink

Dr. P. D. Franzon

Dr. A. Reisman

Dr. E. F. Gehringer

Dr. J. F. Kauffman

(Chair of Advisory Committee)

Biography

Hungying Louis Lo was born in Taipei, Taiwan, on December 20, 1961. In 1984, the author graduated from National Cheng-Kung University, Tainan, Taiwan, with a B.S. degree in Electrical Engineering.

Hungying received an M.S. degree in Electrical Engineering from the University of South Carolina, Columbia, South Carolina, in 1986. In 1986, He entered the Ph.D. program in Electrical and Computer Engineering at North Carolina State University. From 1989 to 1994, he worked in Microelectronic Center North Carolina for electrical design of multi-chip modules, Research Triangle Park, North Carolina.

He is currently a Ph.D. candidate in electrical engineering with minors in Computer Science and Material Science. He married Shuzhi Zhang in 1996.

Acknowledgments

First and foremost, I wish to express my gratitude with my whole heart to my dissertation advisor, Dr. J. Frank Kauffman, for his encouragement and guidance throughout the course of this research. He is always available when I need his help. Without his invaluable guidance and unlimited support, this dissertation would not exist.

I am sincerely grateful to my advisory committee, for their suggestions and advice. I am especially thankful to Dr. Paul Franzon for his encouragement and many valuable discussions. My appreciation also goes to Dr. James Mink for his prompt comments on the research. I thank Dr. Edward Gehringer for his kindly help and allowing me use his computer during the critical time. My appreciation also extends to Dr. Arnold Reisman for serving as a committee member and his kindly help.

I would like to thank Dr. Iwona Turlik for helping me to start the research and supporting me to continue the work.

I would also like to thank North Carolina Supercomputing Center for the research grant and their technique support.

I also thank my colleagues, Dr. Shawkang Wu, Dr. Todd Nuteson, and Huan-sheng Hwang, for many helpful discussions on various parts of this research.

I am also deeply in indebted to my parents for providing me a good environment

to live and grow.

Many great thanks go to my wife, Shuzhi Zhang Lo, for her unreserving support and taking care of me during the time of doing the research.

Finally, I would like to acknowledge God for His everlasting words and unconditional love. Through His grace, I can finish this dissertation.

Contents

| | |
|--|-------------|
| List of Tables | viii |
| List of Figures | ix |
| 1 Introduction | 1 |
| 1.1 Motivation for This Study | 2 |
| 1.2 Original Contributions | 3 |
| 1.3 Dissertation Overview | 4 |
| 2 Literature Review | 6 |
| 2.1 Assumptions | 7 |
| 2.1.1 Quasi-Static Assumption | 7 |
| 2.1.2 Dynamic Assumption | 8 |
| 2.2 Numerical Methods | 8 |
| 2.2.1 Finite-Difference Method and Transmission Line Matrix Method in Time Domain | 8 |
| 2.2.2 Finite Element Method | 9 |
| 2.3 Boundary Conditions | 10 |

| | | |
|----------|---|-----------|
| 2.3.1 | Global Boundary Conditions | 11 |
| 2.3.2 | Local Boundary Conditions | 11 |
| 2.4 | Summary | 12 |
| 3 | Field Calculation by Hybrid Edge/Nodal VFEM | 14 |
| 3.1 | Formula | 15 |
| 3.2 | Propagation Constant | 18 |
| 3.2.1 | Helmholtz's Equation | 19 |
| 3.2.2 | Eigenvalue Problem | 20 |
| 4 | The Three-Component MEI Boundary Condition | 22 |
| 4.1 | Introduction | 22 |
| 4.2 | Theory of MEI Boundary Condition | 23 |
| 4.3 | MEI Boundary Condition for the Electric Field in the Axial Direction | 24 |
| 4.3.1 | The Finite Difference Equation | 26 |
| 4.3.2 | Metrons | 28 |
| 4.4 | MEI Boundary Condition for Transverse Electric Field | 29 |
| 4.4.1 | MEI Cells of Perpendicular-Edge Elements | 31 |
| 4.4.2 | MEI Cells of Parallel-Edge Elements | 32 |
| 5 | Hybrid Edge/Nodal VFEM with Three-Component MEI Boundary Condition | 34 |
| 5.1 | The Matrix Construction for a Small Cell | 35 |
| 5.2 | Vector MEI Boundary Condition for the Elements in the Axial Direction | 41 |
| 5.3 | Vector MEI Boundary Condition for the Elements in Transverse Direction | 42 |

| | | |
|----------|---|-----------|
| 6 | Transmission Loss and Electric Current Distribution in the Conductor | 43 |
| 6.1 | The Triplate Strip Line | 44 |
| 6.2 | The Transmission Line in an MCM | 51 |
| 6.3 | The Coated Interconnection Used in an MCM | 53 |
| 6.3.1 | The Microstrip Clad with Inorganic Dielectric | 54 |
| 6.3.2 | The Microstrip Coated with Chromium | 56 |
| 7 | Summary and Future Directions | 59 |
| 7.1 | Summary | 59 |
| 7.2 | Discussion of Calculated Results | 60 |
| 7.3 | Future Research | 62 |
| | Bibliography | 65 |
| | Appendices | 71 |
| | Appendix A: Acronyms | 71 |
| | Appendix B: Flow Chart of the Computer Program | 72 |
| | Appendix C: Main Program of the Field Calculation | 75 |

List of Tables

| | | |
|-----|---|----|
| 6.1 | The structure parameters for the triplate transmission line | 45 |
| 6.2 | The structure parameters for the transmission line in an MCM manu- factured by SGI | 52 |
| 6.3 | The structure parameters for the clad microstrip | 55 |
| 6.4 | The structure parameters for the Chromium coated microstrip | 57 |

List of Figures

| | | |
|-----|---|----|
| 1.1 | The cross section of a multi-chip module | 2 |
| 3.1 | The 2-dimensional cross section of a stripline with triangular cells for VFEM calculation | 17 |
| 4.1 | The boundary cells for nodal field calculation | 25 |
| 4.2 | The position l on the periphery of the strip conductor | 28 |
| 4.3 | The boundary cells for edge field calculation | 30 |
| 5.1 | The electric field on the edges and nodes of a small triangular cell . . | 35 |
| 6.1 | The cross section of a triplate line | 44 |
| 6.2 | Calculated and measured transmission loss vs frequency | 45 |
| 6.3 | The perfect conductor boundary condition on the cross section of the triplate line | 46 |
| 6.4 | The current density distribution on the cross section of the center strip of the triplate geometry at 2 GHz | 48 |
| 6.5 | The current density distribution on the cross section of the center strip of the triplate geometry at 4 GHz | 49 |

| | | |
|------|--|----|
| 6.6 | The current density distribution on the cross section of the center strip of the triplate geometry at 6 GHz | 50 |
| 6.7 | The cross section of a transmission line in a MCM | 51 |
| 6.8 | The transmission loss vs frequency for the transmission line in an MCM | 53 |
| 6.9 | The transmission line with a thin-film inorganic dielectric. | 54 |
| 6.10 | The transmission loss vs frequency for the microstrip coated with a thin-film inorganic | 56 |
| 6.11 | The transmission line coated with a thin-film chromium. | 57 |
| 6.12 | The transmission loss of a transmission line coated with chromium. . | 58 |
| 7.1 | A discontinuity connecting two transmission lines | 63 |
| B.1 | The flow chart of the computer code | 74 |

Chapter 1

Introduction

With the rapid improvements in integrated circuit (IC) technologies, the interconnections between the ICs are increasingly limiting the performance of VLSI systems. The IC-packaging technologies are also moving from the printed circuit board to the multi-chip module (MCM). The MCM technologies reduce the wire routing length between ICs and increases the complexity of interconnection. The new IC-packaging technologies can improve VLSI system performance, but they are still in need of Computer-Aided Design(CAD) tools to evaluate the best structure of the transmission line in the MCM. In order to calculate the parameters more accurately for CAD tools, we need to calculate the wave propagation in the transmission line in the MCM in terms of the electromagnetic field at high operating frequency and consider conductor loss and dielectric loss as important factors for the propagation performance. All of the acronyms used in this work are defined in Appendix A.

1.1 Motivation for This Study

In order to accommodate the complexity of interconnection and manufacturing technique, the width of the connecting wire is almost the same as the thickness of the wire as shown in Figure 1.1. The cross-section area of the wire is so small that we cannot

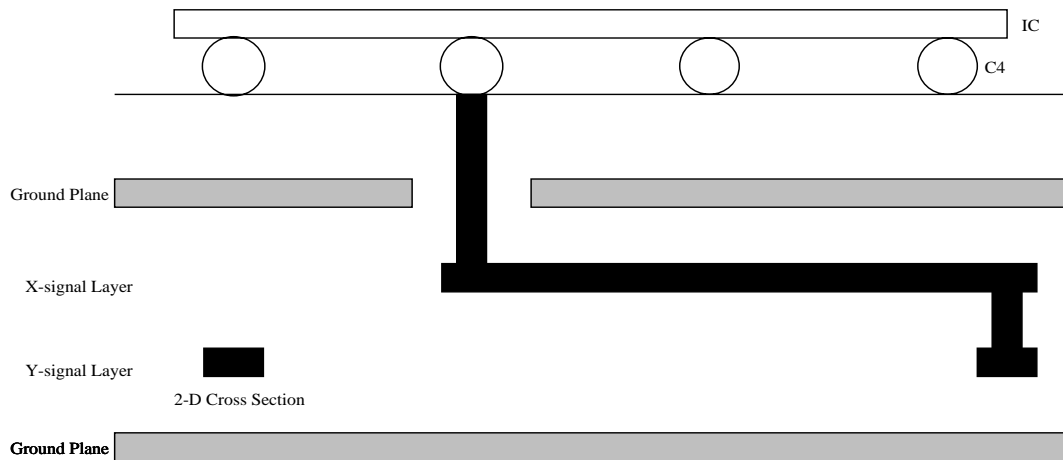


Figure 1.1: The cross section of a multi-chip module

neglect the conductor loss especially for high clock-rate operation. The high speed system needs accurate models to predict system performance and to generate system design rules for the wire routing. Due to the lack of accurate models to optimize the operating performance, the CAD tools on the market for designing the package only apply the limitations of manufacturing technologies and low-frequency circuit models to the rule generation. The manufacturing technologies set up the minimum distance between two connecting wires and the width of the connecting wire to reduce the chance of short circuit or open circuit. The quasi-static assumption and the calculation neglecting the conductor surface charge[37] will not be accurate for high-speed

signals with lossy conductors because their assumptions are based on low operating frequency and low conductor loss. To the best of our knowledge, there is no existing accurate model for the lossy transmission lines within a MCM that enables us to develop design rules and to monitor the signal performance in the MCM.

For the dynamic models, the inductance per unit length, capacitance per unit length, transmission loss, and the characteristic impedance can be calculated from the 3-dimensional electric field distribution on the cross section of the transmission line. We calculate the electromagnetic field distribution for a wave in a transmission line by using the hybrid edge/nodal Vector Finite Element Method (VFEM) with a modified 3-component Measured Equation of Invariance (MEI) boundary condition and predict the lossy propagation constant.

1.2 Original Contributions

- The Measured Equation of Invariance (MEI) boundary condition is modified and applied to hybrid edge/nodal VFEM.
- The three components of the electric field vector on the cross section of the lossy strip conductor of the transmission line are calculated.
- The electromagnetic field distribution, which is a function of the frequency, in the dielectric of a lossy transmission line is calculated.
- The current distribution in the strip conductor of a lossy transmission line is calculated.
- The transmission loss for a transmission line in an MCM is obtained by calcu-

lating the complex propagation constant of the lowest propagation mode.

1.3 Dissertation Overview

A new approach for calculating the electromagnetic field on the cross section of stripline using the hybrid edge/nodal VFEM with a modified MEI boundary condition is described in this dissertation.

Since the cross section of the interconnection conductor inside the MCM is very small and the propagating frequency can be several Giga Hertz (GHz), the loss from the conductor cannot be neglected. Therefore, the edge/nodal VFEM, which is based on dynamic assumption¹, is used to calculate the field distribution inside the conductor.

The MEI boundary condition has only been used for scalar field calculations or 2-dimensional vector field distributions due to a scattering source. We extended the MEI boundary condition to a 3-component vector field calculation for the propagation modes in a realistic thin-film transmission line. The wire thickness is treated as a design parameter, and the conductor loss is an important factor to determine the electromagnetic field distribution.

Chapter 2 reviews the previous work on numerical methods and the boundary conditions for calculating the electromagnetic wave propagation in a transmission line. Various numerical methods are discussed as well as the boundary conditions. The relative merits and shortcomings of these numerical methods and boundary conditions are based on the geometry of the transmission lines.

¹Dynamic assumption is described in section 2.1.2

Chapter 3 describes how the vector Helmholtz equation is used in the hybrid edge/nodal VFEM. The detailed derivation of the eigenvalue matrix equation used for the propagation constant is given. The original contributions begin in Chapter 4 which presents the 3-component MEI boundary condition for vector field distribution calculations. The construction of the matrix equation required for the hybrid edge/nodal VFEM with the 3-component MEI boundary condition is discussed in Chapter 5. Chapter 6 contains the calculation results for different geometries of transmission lines and compares them with the measured data. The summary and possible future research topics are described in Chapter 7. The computer code developed during this study is outlined in Appendix C.

Chapter 2

Literature Review

The characteristics of wave propagation along a transmission line are evaluated by the electromagnetic field distribution over the cross section of the transmission line. Since the propagation characteristics of the signal are very important for designing a multi-chip module (MCM), many efforts have been spent on the calculation. No analytical method has been used to calculate the electromagnetic field distribution on the cross section of a lossy transmission in an MCM, but numerical methods are used to calculate the approximated field distribution. The accuracy of the calculation depends on the assumptions for approximation and the numerical methods used for the calculation. The assumptions for approximation can simplify the problem, but make the calculation applicable only for cases in which the assumptions are not violated. Depending on the calculated structure and the style of output data, the choice of numerical methods plays an important role for computing efficiency and the accuracy of the computed results. For open structures, an artificial boundary condition is often needed for numerical methods to truncate the infinite space.

In this chapter, the assumptions for approximation, the numerical methods, and

the boundary conditions will be reviewed and discussed.

2.1 Assumptions

The electromagnetic field for a propagating wave in a transmission line usually are calculated by making quasi-static assumption or dynamic assumption.

2.1.1 Quasi-Static Assumption

The quasi-static assumption neglects the conductor loss by assuming pure TEM propagation in the transmission line, and the distribution of electromagnetic fields is only in dielectric. The calculation of the electric charge on the surface of the conductor is independent from the calculation of the electric current distribution on the conductor surface, and vice versa. The per-length capacitance[11, 31, 33] or the per-length inductance[24] can be calculated independently by the geometry of the transmission line. Therefore, it is easier to extract the discontinuity effect using the quasi-static assumption. In 1987, Wang, Harrington, and Mautz[35, 36] used the quasi-static assumption to calculate excess capacitance and inductance of a simplified cylindrical via which connects two cylindrical striplines. They assumed that the operating frequency is close to zero and the conductor is a perfect conductor. The propagation modes are assumed to be pure TEM, which is only true for low frequency wave and zero conductor loss. As frequency increases, the electrical dimensions of the structure being analyzed grow larger. The dimensions of the structure are expressed in wavelength. The increase in the electrical dimension of the structure decreases the accuracy of the quasi-static assumption.

2.1.2 Dynamic Assumption

The dynamic assumption is based on the 3-dimensional vector Helmholtz's equation using the medium properties of the materials from which transmission line is made. The electromagnetic field propagation is based on the wave equation specified by the material properties. The propagation modes exist when the electromagnetic field distribution satisfies both Helmholtz's equation and the boundary condition. The calculation of the propagation modes for a lossy transmission line in an MCM should be treated as non-TEM wave propagation by using dynamic assumption because the electric field in the axial direction is not negligible for the small cross-section area of the strip conductor.

2.2 Numerical Methods

Many numerical methods have been developed to analyze the electromagnetic field distribution on the strip line. However, each method is designed for the analysis of a particular type of problem. The calculations of wave propagation in a microstrip transmission line are generally by two classes of methods: time domain, and frequency domain.

2.2.1 Finite-Difference Method and Transmission Line Matrix Method in Time Domain

In order to understand how the wave propagates in a transmission line, the Finite-Difference Time-Domain (FD-TD) method and Transmission Line Matrix (TLM) method can be used to trace how the wave propagates outside the conductor. By

applying an approximate condition that the wavelength, λ , is much larger than the grid dimension l [29], the fundamental formula for both methods are obtained from Maxwell's equations:

$$\nabla \times E = -\mu \frac{\partial H}{\partial t} \quad (2.1)$$

$$\nabla \times H = \sigma E + \epsilon \frac{\partial E}{\partial t} \quad (2.2)$$

The solution to these equations is the field distribution in space under a certain time instant. The input sources are time-sampled analog signals.

The wavelength in the conductor is much smaller than the wavelength in the dielectric area. Therefore, these two time domain methods can only be used to calculate electromagnetic field distribution in the dielectric area, and the conductor is treated as a perfect conductor in which no electromagnetic field exists[18, 30, 39]. In order to obtain the frequency-domain data for CAD tools[13, 38], some authors performed Fourier Transform on the steady-state electromagnetic field distribution calculated by applying sinusoid excitation sources continuously. The computation time needed for the electromagnetic field propagation changing from a transient state to a steady state makes the electromagnetic field calculation very costly. Therefore, these time-domain methods are more often used to graphically illustrate the field propagation than to obtain data for designing an MCM.

2.2.2 Finite Element Method

The calculation in the frequency domain will generate the data directly to be used by CAD tools and without the limit of the grid dimension, which can be larger than the wavelength for the electromagnetic field distribution in a lossy conductor. Finite element method (in frequency domain) is the most versatile method[17] for calculating

the field distribution in the irregular shape dielectric and conductors compared to other numerical methods (finite difference method, TLM method, etc.). Since the cross section of an interconnection path inside the MCM is small and the propagating frequency can be several Giga Hertz(GHz), the loss from the conductor cannot be neglected. Because the transmission loss is mainly from the conductor, VFEM is a good choice to calculate the electromagnetic field distribution on the cross section of a lossy transmission line.

In 1992, Koshiha and Inoue[14] proposed a VFEM with hybrid edge/nodal elements to calculate the electric field on the cross section of a lossy strip line in an MCM. Their method rigorously evaluates propagation characteristics of a lossy transmission line, but they used a perfect conductor as the outer boundary condition of the VFEM calculated volume for an open structure. Many layers of elements are required between the conductor surface and the perfect conductor boundary condition for reducing the error caused by the truncation of the field distribution on the perfect-conductor boundary condition. Because of limited computer memory, the published papers showed only the transmission loss of the transmission line without showing the field distribution in the conductor. If a better boundary condition can be applied to the calculation by VFEM, the field distribution can be calculated more accurately for wave propagation in a transmission line.

2.3 Boundary Conditions

Due to the limits of computer memory, the finite element method cannot be used to calculate the field distribution in an open area unless we put an artificial boundary condition to limit the calculated area. The published boundary conditions are in

two categories: local boundary conditions, and global boundary conditions. The choice of the boundary conditions for numerical calculation affects the accuracy of the calculated results and affects the amount of resources (computing time and hardware memory) needed for the calculation.

2.3.1 Global Boundary Conditions

The global boundary conditions either make the outer-boundary elements fully coupled by using a series of matrix calculations for keeping the electromagnetic wave outgoing on the boundary[32] or generate external layers of elements, which are full coupled with inner elements, to have the electromagnetic wave continuously distributed to the boundary and out to infinite space[19]. The advantage of global conditions is that the boundary can be placed very close to the conductor surface, then the size of grid matrix for inner elements will be small. There are two main disadvantages for global conditions. First, the calculation for the coupling matrix between inner elements and outer elements is almost the amount of calculation for solving the whole matrix equation. Second, the grid matrix will be much denser than the the grid matrix by using local boundary conditions.

2.3.2 Local Boundary Conditions

The local boundary conditions consist of local operators or finite difference equations to absorb the outgoing electromagnetic wave on the boundary or to simulate the infinite space for the wave excited from the conductor surface. These boundary elements are not coupling with the inner elements. Several layers of elements are needed to buffer between the conductor surface and the boundary elements in order

to reduce the incident angle on the artificial boundary for the electromagnetic field induced from the current distribution on the conductor surface[27, 28]. In 1994, Mei et al.[20] proposed a rigorous local method, the Measured Equation of Invariance (MEI) method, to model the boundary condition of an open structure for finite element method or finite difference method. It is based on the concept that the local finite difference equations can be written at boundary nodes with the geometry information being incorporated into the equations. The MEI method allows one to place the FEM boundary very close to the conductor surface; thereby more computer memory is available to calculate the field distribution inside the lossy conductor.

2.4 Summary

In order to calculate the electromagnetic field distribution accurately with limited computer resources, it is very important to choose an efficient numerical method with a suitable boundary condition to truncate the infinite space. The loss from the strip conductor in an MCM causes the electric field to be induced in the axial direction. Therefore, the field distribution for a wave propagation along a transmission line in an MCM needs to be calculated by making dynamic assumption due to the conducting loss. The hybrid edge/nodal VFEM is designed to handle the lossy microstrip in an MCM, but the perfect conductor boundary condition which just assigns zero field on the boundary was used for this numerical method. Although the global boundary conditions can couple the finite element method well, the eigenvalue equation in the hybrid edge/nodal VFEM is not compatible with the global boundary conditions. The MEI boundary condition can be placed very close to the conductor without affecting the accuracy, but prior to this work it was used only for calculating 2-dimensional

scattering of a TE or TM waves. The goal of this work is to calculate the transmission loss of a high speed transmission line by using 3-component MEI boundary condition for the the hybrid edge/nodal VFEM.

Chapter 3

Field Calculation by Hybrid Edge/Nodal VFEM

By using the VFEM with edges and nodes in each mesh cell, the complex propagation constant can be calculated along with the distribution of the electromagnetic field on the transverse plane and in the axial direction. The hybrid edge/nodal VFEM is a rigorous method in calculating the propagation modes for a lossy transmission line, but the method is lacking a proper boundary condition to reduce a calculated area for electromagnetic field distribution. Using a perfect conductor wall as the boundary condition[3] requires the calculated area large enough to cover the ground plate. Because of limited computer memory, the boundary condition is forced to be placed close to the conductor surface, and the partition for the cross section of the conductor strip is very coarse. Therefore, the hybrid edge/nodal VFEM with perfect conductor wall as its boundary condition cannot accurately calculate the current distribution in the loss conductor and predict the transmission loss.

In order to explain more clearly how the hybrid edge/nodal VFEM can be used

to calculate the propagation modes of a lossy transmission line, we will describe the method without the boundary condition in this chapter. Because we want to see how the current is distributed in the conductor, the electric field distribution is used as the variable for the Helmholtz's equation to be solved by using the hybrid edge/nodal VFEM.

3.1 Formula

In a source-free lossy medium, the homogeneous vector Helmholtz's equation for the electric field is

$$\nabla \times (\nabla \times \vec{E}) - k_c^2 \vec{E} = 0 \quad (3.1)$$

where the wave number k_c is a complex number for the conducting region,

$$\begin{aligned} k_c &= \omega \sqrt{\mu_c \epsilon_c} \\ &= \omega \sqrt{\mu_r \mu_0 \hat{\epsilon}_r \epsilon_0} \end{aligned} \quad (3.2)$$

where μ_r is the relative permeability of the region of interest, $\hat{\epsilon}_r$ is the complex relative permittivity of the region of interest, μ_0 and ϵ_0 are the permeability and permittivity in free space. Substituting Equation (3.2) into Equation (3.1), we get the vector Helmholtz's equation

$$\nabla \times (\nabla \times \vec{E}) - k_0^2 \mu_r \hat{\epsilon}_r \vec{E} = 0 \quad (3.3)$$

where k_0 is the wave number in free space, and it equals to $\omega \sqrt{\mu_0 \epsilon_0}$.

For a conductor, the electric field and the magnetic field are related according to the time-harmonic Maxwell's equation,

$$\begin{aligned}
\nabla \times \vec{H} &= \vec{J} + j\omega\epsilon_0\vec{E} \\
&= \sigma\vec{E} + j\omega\epsilon_0\vec{E} \\
&= (\sigma + j\omega\epsilon_0)\vec{E} \\
&= j\omega(1 - j\frac{\sigma}{\omega\epsilon_0})\epsilon_0\vec{E}
\end{aligned} \tag{3.4}$$

where \vec{J} is the density of the conduction current, σ is the conductivity of the conductor, and ω is the radian frequency. In order to simplify Equation (3.4), we define the complex relative permittivity of a conductor as

$$\hat{\epsilon}_r = 1 - j\frac{\sigma}{\omega\epsilon_0} \tag{3.5}$$

and for a lossy dielectric it can be written as

$$\hat{\epsilon}_r = \epsilon_r (1 - j \tan \delta) \tag{3.6}$$

where ϵ_r is the relative permittivity of the dielectric, and $\tan \delta$ is the loss tangent. For a lossless dielectric, the loss tangent is zero. The VFEM functional of the Helmholtz's equation on the 2-dimensional cross section is given by

$$\begin{aligned}
F &= \iint_{\Omega} [(\nabla \times (\nabla \times \vec{E}) - k_0^2\mu_r\hat{\epsilon}_r\vec{E}) \cdot \vec{E}^*] dx dy \\
&= \iint_{\Omega} [(\nabla \times \vec{E}) \cdot (\nabla \times \vec{E})^* - k_0^2\mu_r\hat{\epsilon}_r\vec{E} \cdot \vec{E}^*] dx dy,
\end{aligned} \tag{3.7}$$

where Ω is the calculated area on the cross-section plane, and the superscript $*$ means the complex conjugate.

In order to apply VFEM to the field calculation, we assign a number of hybrid edge/nodal triangular cells to cover the cross section of the strip conductor in the

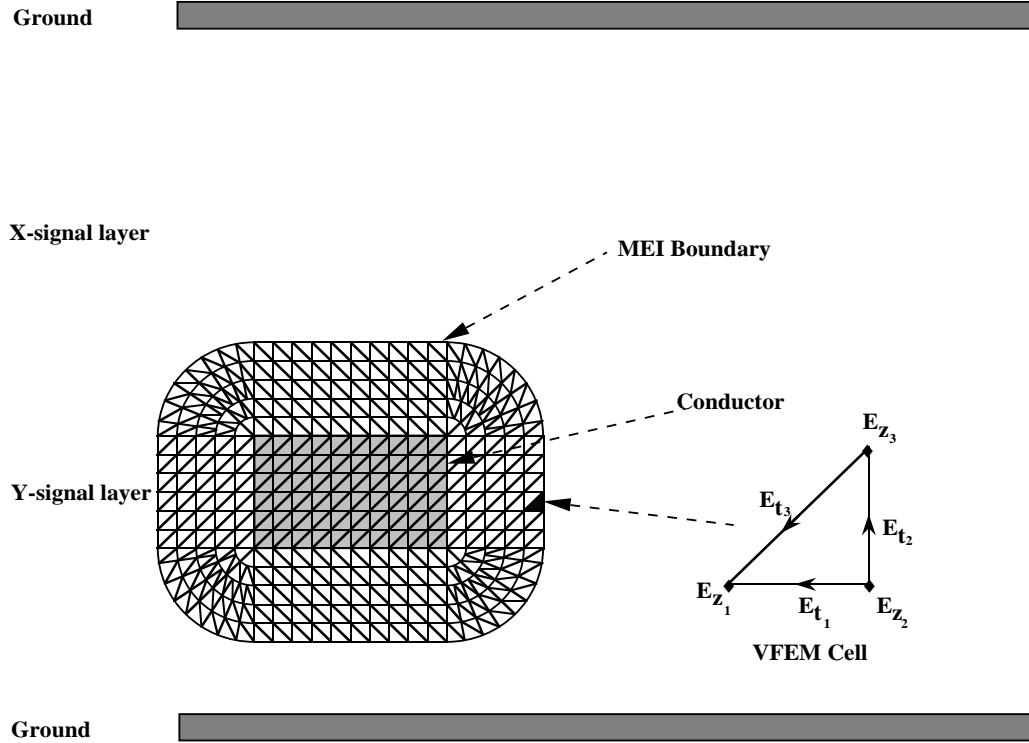


Figure 3.1: The 2-dimensional cross section of a stripline with triangular cells for VFEM calculation

bottom left corner of Figure 1.1, and the partition is illustrated in Figure 3.1. The edge elements, $\{E_t\}$, of the VFEM cell on the right-hand side of Figure 3.1 are \vec{E}_{t_1} , \vec{E}_{t_2} , and \vec{E}_{t_3} . The node elements, $\{E_z\}$, of the cell are \vec{E}_{z_1} , \vec{E}_{z_2} , and \vec{E}_{z_3} . The distribution of the electric field in the x, y, and z directions for the enclosed area of

each cell is determined by the field strength of the edge/node elements in the cell as

$$E = \begin{bmatrix} E_x \\ E_y \\ E_z \end{bmatrix} = \begin{bmatrix} \{U\}^T \{E_t\}_e \\ \{V\}^T \{E_t\}_e \\ j\{N\}^T \{E_z\}_e \end{bmatrix} \quad (3.8)$$

where $\{U\}$ and $\{V\}$ are the shape-function sets for the edge elements, $\{N\}$ is the shape-function set for the node elements, T is the transpose operator for the vector, and j is the square root of -1 . The factor j is used to time the shape function of node elements, because the field in the axial direction is orthogonal to the field in the transverse direction.

3.2 Propagation Constant

We take γ as the complex propagation constant. The derivative of the shape functions in the axial direction for each small cell in Figure 3.1 is γ times the shape function. The real part of the complex propagation constant is the attenuation constant. The transmission loss (dB/mm) is related to the attenuation constant $\alpha(\text{m}^{-1})$ by

$$\begin{aligned} \text{Transmission Loss (dB/mm)} &= -\log_{10} e^{-2\alpha} \\ &= 2\alpha \log_{10} e^1 \\ &= 8.69 \times 10^{-4} \alpha(\text{m}^{-1}) \end{aligned} \quad (3.9)$$

Therefore, the transmission loss (dB/mm) equals the attenuation constant, $\alpha(\text{m}^{-1})$, times 8.69×10^{-4} .

3.2.1 Helmholtz's Equation

In order to derive the Helmholtz's equation in terms of the complex propagation constant and the shape function, we take the curl of \vec{E} given by Equation (3.8),

$$\begin{aligned}
\nabla \times \vec{E} &= \nabla \times \left(\{U\}^T \{E_t\}_e, \{V\}^T \{E_t\}_e, j\{N\}^T \{E_z\}_e \right) \\
&= \left(j\{E_z\}_e^T \frac{\partial \{N\}}{\partial y} - \{E_t\}_e^T \frac{\partial \{V\}}{\partial z}, \{E_t\}_e^T \frac{\partial \{U\}}{\partial z} - j\{E_z\}_e^T \frac{\partial \{N\}}{\partial x}, \right. \\
&\quad \left. \{E_t\}_e^T \frac{\partial \{V\}}{\partial x} - \{E_t\}_e^T \frac{\partial \{U\}}{\partial y} \right) \\
&= \left(j\{E_z\}_e^T \frac{\partial \{N\}}{\partial y} + j\gamma \{E_t\}_e^T \{V\}, -j\gamma \{E_t\}_e^T \{U\} - j\{E_z\}_e^T \frac{\partial \{N\}}{\partial x}, \right. \\
&\quad \left. \{E_t\}_e^T \frac{\partial \{V\}}{\partial x} - \{E_t\}_e^T \frac{\partial \{U\}}{\partial y} \right) \quad (3.10)
\end{aligned}$$

and represent $E \cdot E^*$ in terms of shape functions as

$$E \cdot E^* = \{U\}^T \{U\} \{E_t\}^T \{E_t\}^* + \{V\}^T \{V\} \{E_t\}^T \{E_t\}^* + \{N\}^T \{N\} \{E_z\}^T \{E_z\}^* \quad (3.11)$$

where the superscript $*$ means the complex conjugate of the vector.

Substituting Equation (3.10) and Equation (3.11) into Equation (3.7), we get the functional of the Helmholtz's equation in terms of shape functions and edge/nodal elements as

$$\begin{aligned}
F &= \iint_{\Omega} -\gamma^2 \left[\left(\{U\}^T \{U\} + \{V\}^T \{V\} \right) \{E_t\}^T \{E_t\}^* \right. \\
&\quad - \gamma \left(\{U\}^T \{N_x\} + \{U\}^T \{N_x\} \right) \{E_t\}^T \{E_z\}^* \\
&\quad - \gamma \left(\{U\}^T \{N_x\} + \{U\}^T \{N_x\} \right) \{E_z\}^T \{E_t\}^* \\
&\quad + (U_y - V_x)^T (V_x - U_y) \{E_t\}^T \{E_t\}^* \\
&\quad - k_0^2 \mu_r \vec{e}_r \left(\{U\}^T \{U\} + \{V\}^T \{V\} \right) \{E_t\}^T \{E_t\}^* \\
&\quad \left. - k_0^2 \mu_r \vec{e}_r \{N\}^T \{N\} \{E_z\}^T \{E_z\}^* \right] dx dy \quad (3.12)
\end{aligned}$$

In order to get the electric field distribution on the finite element edges, we substitute Equation (3.8) into (3.7), and minimize the VFEM functional by

$$\frac{\partial F}{\partial E_i} = 0, i = 1, 2, 3, \dots, N \quad (3.13)$$

where N is the total number of edges. This results in the following matrix equation:

$$\begin{bmatrix} [K_{tt}] - \gamma^2 [M_{tt}] & -\gamma [K_{tz}] \\ -\gamma [K_{zt}] & [K_{zz}] \end{bmatrix} \begin{bmatrix} \{E_t\} \\ \{E_z\} \end{bmatrix} = \begin{bmatrix} \{0\} \\ \{0\} \end{bmatrix} \quad (3.14)$$

with

$$\begin{aligned} [K_{tt}] &= \sum_e \iint_e [\hat{\epsilon}_r k_0^2 \{U\}^T \{U\} + \hat{\epsilon}_r k_0^2 \{V\}^T \{V\}] dx dy \\ &+ \sum_e \iint_e [(\{U_y\}^T - \{V_x\}^T) (\{V_x\} - \{U_y\})] dx dy \end{aligned} \quad (3.15)$$

$$[K_{tz}] = \sum_e \iint_e [\{U\}^T \{N_x\} + \{V\}^T \{N_y\}] dx dy = [K_{zt}] \quad (3.16)$$

$$[K_{zz}] = \sum_e \iint_e [\hat{\epsilon}_r k_0^2 \{N\}^T \{N\} - \{N_x\}^T \{N_x\} - \{N_y\}^T \{N_y\}] dx dy \quad (3.17)$$

$$[M_{tt}] = \sum_e \iint_e [\{U\}^T \{U\} + \{V\}^T \{V\}] dx dy \quad (3.18)$$

where $\{U_y\} \equiv \partial\{U\}/\partial y$, $\{V_x\} \equiv \partial\{V\}/\partial x$, $\{N_x\} \equiv \partial\{N\}/\partial x$, and $\{N_y\} \equiv \partial\{N\}/\partial y$.

3.2.2 Eigenvalue Problem

Separating the electric field strength into transverse and axial components in Equation (3.14), we get the following matrix equations:

$$-[K_{tt}] \{E_t\} + \gamma [K_{tz}] \{E_z\} + \gamma^2 [M_{tt}] \{E_t\} = \{0\} \quad (3.19)$$

$$\gamma [K_{zt}] \{E_t\} - [K_{zz}] \{E_z\} = \{0\} \quad (3.20)$$

Eliminating the axial component from these two matrix equations, we get the following equation which is solved for γ .

$$[K_{tt}] \{E_t\} - \gamma^2 \left([K_{tz}] [K_{zz}]^{-1} [K_{zt}] + [M_{tt}] \right) \{E_t\} = \{0\} \quad (3.21)$$

In order to find out the propagation mode of Equation (3.21), we rewrite it as

$$A \{E_t\} - \lambda B \{E_t\} = \{0\} \quad (3.22)$$

with

$$\begin{aligned} A &= [K_{tt}] \\ B &= [K_{tz}] [K_{zz}]^{-1} [K_{zt}] + [M_{tt}] \\ \lambda &= \gamma^2. \end{aligned}$$

where γ is the complex propagation constant. Let $B \{E_t\} = y$, then $\{E_t\} = B^{-1}y$. Substituting $B \{E_t\}$ by y , and $\{E_t\}$ by $B^{-1}y$ in Equation (3.22), we get

$$AB^{-1}y - \lambda y = \{0\} \quad (3.23)$$

Assigning $M = AB^{-1}$, we get an eigenvalue equation

$$My = \lambda y. \quad (3.24)$$

Since the matrix M is not sparse, we have no choice but to use a dense-matrix solver (QR decomposition) for calculating the complex eigenvalue. The solutions for the eigenvalues, $\lambda = \gamma^2$, in the eigenvalue equation represent the propagation modes. By substituting the eigenvalue of the dominant propagation mode back into Equation (3.21), we calculate the transverse electric field distribution on the cross section of the stripline. The electric field distribution in the axial direction is calculated by substituting the eigenvalue of the dominant propagation mode and the transverse electric field distribution, $\{E_t\}$, into Equation (3.20).

Chapter 4

The Three-Component MEI Boundary Condition

4.1 Introduction

The MEI boundary condition is a local boundary condition for both the finite element method and finite difference method. This boundary condition was originally used for 2-dimensional scattering of a transverse electric wave or a transverse magnetic wave[20, 8]. In this dissertation, the theory of the MEI boundary condition is extended to the boundary condition for the hybrid edge/nodal VFEM for calculating the electric field distribution of a propagating wave in a transmission line in an MCM.

The MEI boundary condition is based on a linear finite difference equation for determining the electric field distribution on the boundary element. Because the MEI boundary condition incorporates the conductor geometry into the finite difference equation, the boundary condition can be placed very close to the conductor surface without sacrificing accuracy. The small calculated area for the numerical method

with MEI boundary condition will reduce the size of the matrix equation for the calculation. Therefore, the current density distribution on the cross section contour of the conductor can be calculated with limited computer resources.

On the artificial boundary, the field in transverse direction can be calculated independently from the field in the axial direction by using the 3-component MEI boundary condition. If we apply a global boundary condition to the matrix equations for hybrid edge/nodal VFEM calculation, the dependency between the transverse elements and the axial elements will make the calculation of the eigenvalue very difficult. Therefore, the global boundary conditions are not suitable for the edge/nodal VFEM calculation.

4.2 Theory of MEI Boundary Condition

The MEI boundary condition uses a finite difference equation to describe how the electromagnetic field distribution on a boundary element relates to the field distribution on the neighboring elements. The finite difference equation is given as:

$$\sum_{i=0}^{n-1} a_i \phi_i = 0 \quad (4.1)$$

where $i = 0$ corresponds to the boundary element and $i=1, i=2, \dots, i=n-1$ correspond to the neighboring elements. Let $a_0 = -1$, and the coefficients a_1, \dots, a_{n-1} are determined by applying $n - 1$ distributions (called metrons)[20] of surface current density on the conductor. The field distribution on the boundary element is determined by Equation (4.1) instead of by the mesh equation from the numerical method. The theory of MEI boundary condition is based on three postulates:

Postulate 1 The coefficients of Equation (4.1) are location dependent.

Postulate 2 The coefficients of Equation (4.1) are geometry specific.

Postulate 3 The coefficients of Equation (4.1) are approximately invariant with excitation.

Postulates 1 and 2 explain why we can use MEI boundary to replace the whole outer space. Postulate 3 enables us to replace the outer boundary of FDM/FEM mesh cells by MEI cells as shown in Figure 4.1.

4.3 MEI Boundary Condition for the Electric Field in the Axial Direction

In order to calculate the field distribution on the boundary nodes of the FEM mesh, eight-node cells are used as shown in Figure 4.1. The axial component of the electric field outside the conductor is related to the electric current density in the conductor by the following relation

$$\vec{E} = j\omega\vec{A} \quad (4.2)$$

with

$$\vec{A} = \frac{\mu_0}{4\pi} \int_S G(\vec{r}|\vec{r}') J(\vec{r}') d\vec{r}' \quad (4.3)$$

where S is the cross section of the conductor, μ_0 is the free space permeability, and $G(\vec{r}|\vec{r}')$ is the Green's function.

The direction of the electric field on each node is perpendicular to the cross-section plane of the strip conductor, and the electric field on the nodes of a boundary cell is related to the axial component of the current density distribution in the conductor. By using a finite difference equation to represent the relationship of the field distribution

on the nodes in a MEI cell, the field distribution on the boundary node is determined by the field distribution on its neighboring nodes.

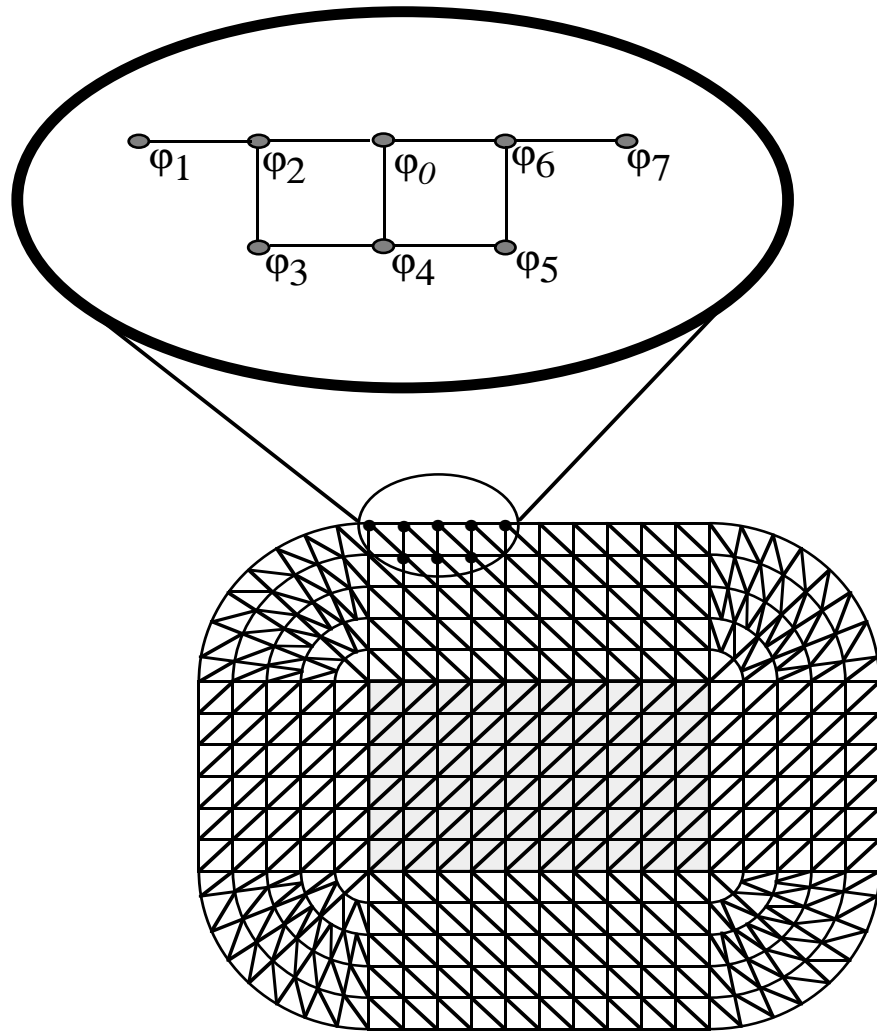


Figure 4.1: The boundary cells for nodal field calculation

4.3.1 The Finite Difference Equation

For the eight-node MEI cells shown in Figure 4.1, the axial component of electric field on node 0, E_0 , is determined by the following finite difference equation,

$$a_1 E_1 + a_2 E_2 + a_3 E_3 + a_4 E_4 + a_5 E_5 + a_6 E_6 + a_7 E_7 = E_0, \quad (4.4)$$

where a_1, \dots, a_7 are the coefficients of the finite difference equation, and the values must be calculated for each MEI cell. The variables E_0, \dots, E_7 are the axial components of electric field on the nodes in a MEI cell, and their values are calculated by the axial component of current density distribution in the conductor. By using the Equivalence Principle[12], the effect of the current density distribution inside the conductor can be replaced by a current density distribution on the conductor surface. For an assigned current density distribution (*metron k*) on the surface of the conductor, the axial component of electric field distribution on node i is

$$E_i^k(\vec{r}) = \oint_C G(\vec{r}|\vec{r}') J_z^k(\vec{r}') d\vec{r}', \quad (4.5)$$

where C is the contour of the conductor, $J_z^k(\vec{r}')$ is the surface current density of *metron k* at point \vec{r}' on the surface of the conductor, and $G(\vec{r}|\vec{r}')$ is the Green's function. For the infinite transmission line, the Green's function is the Hankel function of zero order and second kind[8].

Seven metrons are needed to derive the coefficients a_1, \dots, a_7 in Equation (4.4). The electric field distribution on node 0, node 1, ..., node 7 is calculated by Equation (4.5) for each assigned metron. After substituting the electric field on the nodes in Equation (4.4) by applying seven different metrons, *metron 0, ..., metron 6* on the conductor surface, we get the following 7 equations:

$$\begin{aligned}
\text{metron } 0 &\Rightarrow a_1 E_1^0 + a_2 E_2^0 + a_3 E_3^0 + a_4 E_4^0 + a_5 E_5^0 + a_6 E_6^0 + a_7 E_7^0 = E_0^0 \\
\text{metron } 1 &\Rightarrow a_1 E_1^1 + a_2 E_2^1 + a_3 E_3^1 + a_4 E_4^1 + a_5 E_5^1 + a_6 E_6^1 + a_7 E_7^1 = E_0^1 \\
\text{metron } 2 &\Rightarrow a_1 E_1^2 + a_2 E_2^2 + a_3 E_3^2 + a_4 E_4^2 + a_5 E_5^2 + a_6 E_6^2 + a_7 E_7^2 = E_0^2 \\
\text{metron } 3 &\Rightarrow a_1 E_1^3 + a_2 E_2^3 + a_3 E_3^3 + a_4 E_4^3 + a_5 E_5^3 + a_6 E_6^3 + a_7 E_7^3 = E_0^3 \\
\text{metron } 4 &\Rightarrow a_1 E_1^4 + a_2 E_2^4 + a_3 E_3^4 + a_4 E_4^4 + a_5 E_5^4 + a_6 E_6^4 + a_7 E_7^4 = E_0^4 \\
\text{metron } 5 &\Rightarrow a_1 E_1^5 + a_2 E_2^5 + a_3 E_3^5 + a_4 E_4^5 + a_5 E_5^5 + a_6 E_6^5 + a_7 E_7^5 = E_0^5 \\
\text{metron } 6 &\Rightarrow a_1 E_1^6 + a_2 E_2^6 + a_3 E_3^6 + a_4 E_4^6 + a_5 E_5^6 + a_6 E_6^6 + a_7 E_7^6 = E_0^6
\end{aligned}$$

where E_i^j , calculated by Equation (4.5), is the electric field intensity on node i due to *metron* j . These equations can be rewritten as a matrix form,

$$\begin{bmatrix} E_1^1 & E_2^1 & E_3^1 & E_4^1 & E_5^1 & E_6^1 & E_7^1 \\ E_1^2 & E_2^2 & E_3^2 & E_4^2 & E_5^2 & E_6^2 & E_7^2 \\ E_1^3 & E_2^3 & E_3^3 & E_4^3 & E_5^3 & E_6^3 & E_7^3 \\ E_1^4 & E_2^4 & E_3^4 & E_4^4 & E_5^4 & E_6^4 & E_7^4 \\ E_1^5 & E_2^5 & E_3^5 & E_4^5 & E_5^5 & E_6^5 & E_7^5 \\ E_1^6 & E_2^6 & E_3^6 & E_4^6 & E_5^6 & E_6^6 & E_7^6 \\ E_1^7 & E_2^7 & E_3^7 & E_4^7 & E_5^7 & E_6^7 & E_7^7 \end{bmatrix} \begin{bmatrix} a_1 \\ a_2 \\ a_3 \\ a_4 \\ a_5 \\ a_6 \\ a_7 \end{bmatrix} = \begin{bmatrix} E_0^1 \\ E_0^2 \\ E_0^3 \\ E_0^4 \\ E_0^5 \\ E_0^6 \\ E_0^7 \end{bmatrix}. \quad (4.6)$$

The coefficients a_1, \dots, a_7 can be determined by solving Equation (4.6). Therefore, the electric field distribution on node 0 is determined by Equation (4.4), and this boundary condition is used to truncate the infinite space outside the calculated area.

4.3.2 Metrons

In order to solve the coefficients, a_1 to a_7 , in Equation (4.4), seven different metrons of current density distribution on the conductor surface are needed. We define the length of the cross-section contour of the conductor strip as L and the point on the cross-section contour of the strip is l as shown in Figure 4.2. Because the metron and the space derivative of the metron need to be continuous functions[23], the seven distributions of surface current density in the axial direction are assigned as sinusoidal distributions:

$$J_z^k(l) = \begin{cases} \cos \frac{2k\pi l}{L}, & k = 0, 1, 2, 3 \\ \sin \frac{2(k-3)\pi l}{L}, & k = 4, 5, 6 \end{cases} \quad (4.7)$$

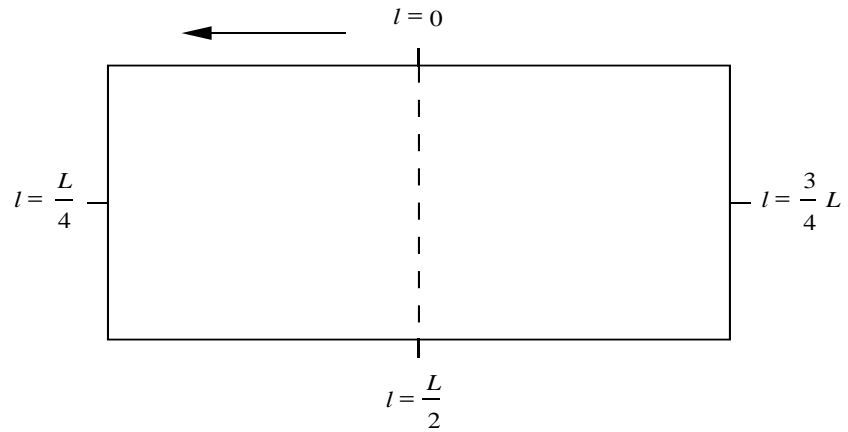


Figure 4.2: The position l on the periphery of the strip conductor

The axial current density on the conductor surface can be approximated by a summation of Fourier series:

$$\begin{aligned}
 J_s &= \sum_{k=0}^3 b_k \cos \frac{2k\pi l}{L} + \sum_{k=4}^6 b_k \sin \frac{2(k-3)\pi l}{L} \\
 &= \sum_{k=0}^6 b_k J_z^k(l)
 \end{aligned} \tag{4.8}$$

The residuals of the MEI boundary equations for the the current distribution of the sinusoidal components in Equation (4.8) are zero because we use these terms to evaluate the finite difference equation for the boundary condition. Using additional terms does not improve the accuracy as it does with some numerical methods such as the method of moments. This is because of Postulates 2 in Section 4.2. The use of the geometry specific Green's function for the metrons to calculate the coefficients of the finite difference equation makes the use of addition terms unnecessary. MEI and et al.[20] have shown that the residuals of the boundary equations are almost zero for additional terms in the summation of Equation (4.8).

4.4 MEI Boundary Condition for Transverse Electric Field

On the transverse plane, the electric field inside the conductor is dependent only upon the transverse current density in the conductor, but the electric field outside the conductor is dependent upon both the surface charge density on the conductor and the surface current density on the transverse plane. On the surface of the conductor, the direction of the electric field vector due to the surface charge density is perpendicular to the conductor surface, and the electric field due to the surface current density is parallel to the conductor surface. The edge elements of the numerical mesh in

the dielectric are used to define the two orthogonal field components: the electric field perpendicular to the artificial boundary, and the electric field parallel to the artificial boundary. Because the MEI boundary is placed very close to the conductor surface, the boundary condition for the electric field due to the surface charge density is modeled using the MEI cells with perpendicular-edge elements, and the boundary condition for the electric field due to the surface current density on the transverse plane is modeled using MEI cells with parallel-edge elements as shown in Figure 4.3.

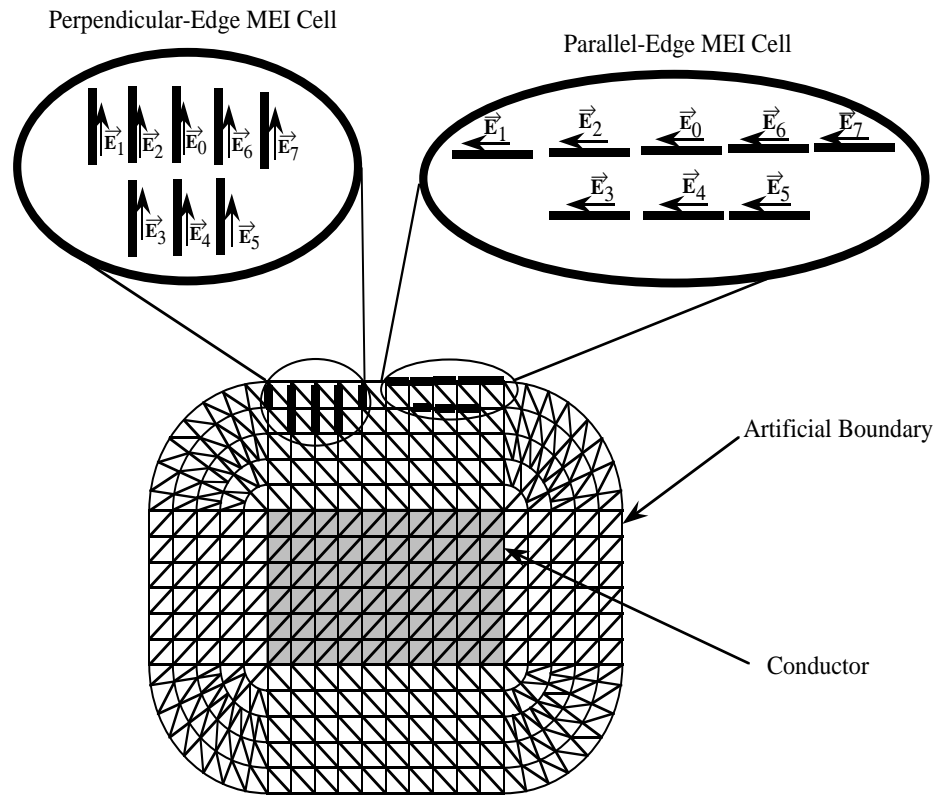


Figure 4.3: The boundary cells for edge field calculation

4.4.1 MEI Cells of Perpendicular-Edge Elements

For a perpendicular-edge MEI cell in Figure 4.3, the electric field \vec{E}_0 on the perpendicular-edge element 0 is determined by the following finite difference equation,

$$a_1 \vec{E}_1 + a_2 \vec{E}_2 + a_3 \vec{E}_3 + a_4 \vec{E}_4 + a_5 \vec{E}_5 + a_6 \vec{E}_6 + a_7 \vec{E}_7 = \vec{E}_0, \quad (4.9)$$

where the coefficients, a_1, \dots, a_7 are calculated by applying 7 metrons on the surface of the conductor. The metrons of the surface charge density on the cross-section contour of the conductor in Figure 4.2 are assigned as

$$Q_s^k(l) = \begin{cases} \cos \frac{2k\pi l}{L}, & k = 0, 1, 2, 3 \\ \sin \frac{2(k-3)\pi l}{L}, & k = 4, 5, 6 \end{cases} \quad (4.10)$$

where k is the metron number.

The electric field intensity on perpendicular-edge element i in Figure 4.3 is due to the surface charge *metron* k as:

$$\begin{aligned} \vec{E}_i^k(\vec{r}) &= [\nabla V_i^k(\vec{r})] \cdot \hat{s}_i \\ &= \nabla \left[\frac{1}{4\pi\epsilon_r\epsilon_0} \oint_C G(\vec{r}|\vec{r}') Q_s^k(\vec{r}') d\vec{r}' \right] \cdot \hat{s}_i, \end{aligned} \quad (4.11)$$

where $V_i^k(\vec{r})$ is the electric potential on the perpendicular-edge element i , $Q_s^k(r')$ is the electric charge density on the conductor surface for *metron* k , ϵ_r is relative permittivity, ϵ_0 is the permittivity in free space, and \hat{s}_i is a unit vector on edge i , whose direction is toward the artificial boundary.

After seven metrons in Equation (4.10) are applied to the finite difference equation (4.9) for a perpendicular-edge MEI cell, the coefficients of the MEI cells can be solved as described in section 4.3. By the same argument for eight-node MEI cells, the electric field on the perpendicular-edge element 0 is determined by the finite difference

equation (4.9) for the perpendicular-edge boundary condition. By the same token, the electric field on each perpendicular-edge element on the artificial boundary is determined by the finite difference equation calculated from the MEI cell of this boundary element instead of the mesh equation from FEM.

4.4.2 MEI Cells of Parallel-Edge Elements

For the parallel-edge MEI cells in Figure 4.3, the parallel-edge element 0 is determined by the following finite difference equation,

$$a_1 \vec{E}_1 + a_2 \vec{E}_2 + a_3 \vec{E}_3 + a_4 \vec{E}_4 + a_5 \vec{E}_5 + a_6 \vec{E}_6 + a_7 \vec{E}_7 = \vec{E}_0, \quad (4.12)$$

where the coefficients, a_1, \dots, a_7 are calculated by applying 7 metrons of transverse current density on the surface of the conductor. The metrons of the surface current density on the cross section of the conductor in Figure 4.2 are assigned as

$$J_s^k(l) = \begin{cases} \cos \frac{2k\pi l}{L}, & k = 0, 1, 2, 3 \\ \sin \frac{2(k-3)\pi l}{L}, & k = 4, 5, 6 \end{cases} \quad (4.13)$$

where k is the metron number.

The electric field intensity on the parallel-edge element i from a metron is calculated by

$$\vec{E}_i^k(\vec{r}) = \oint_C G(\vec{r}|\vec{r}') \vec{J}_s^k(\vec{r}') \cdot \hat{s}_i dr', \quad (4.14)$$

where \hat{s}_i is the unit vector on edge i , whose direction is counterclockwise and parallel to the artificial boundary, and $\vec{J}_s^k(\vec{r}')$ is the conductor surface current density on the transverse plane for *metron* k .

After seven metrons in Equation (4.13) are applied to the finite difference equation of the parallel-edge MEI cell, the coefficients of the MEI cells can be solved as

described in section 4.3. Therefore, the electric field intensity on the parallel-edge element 0 is determined by the Equation (4.12) for the parallel-edge boundary condition. By the same token, the electric field on each parallel-edge element on the boundary is determined by the finite difference equation calculated from the MEI cell of this boundary element instead of the mesh equation from FEM.

Chapter 5

Hybrid Edge/Nodal VFEM with Three-Component MEI Boundary Condition

In order to reduce the number of the calculated elements in the dielectric to save computer memory and time, we apply the 3-component MEI boundary condition[20] for the field distribution on the outer VFEM elements. The local finite difference equation is used at the boundary elements in the matrix equation. For the propagation modes in the transmission line, the concept of MEI boundary condition makes the calculation more efficient and accurate.

In this chapter, the construction of the matrix equations used in the hybrid edge/nodal VFEM is described in detail. How the 3-component MEI boundary condition being used for the eigenvalue equation is also explained.

5.1 The Matrix Construction for a Small Cell

The calculated area consists of small cells for the hybrid edge/nodal VFEM calculation. The electric field inside each small cell is represented by a shape-function matrix times the electric field on the nodes and edges. The construction of the matrices in Equation (3.13) is the summation of the shape-function matrices for all the small cells by the relation of the vector Helmholtz's equation. The first step to construct the matrices is to calculate the shape functions and the derivatives of the shape functions of the elements in a small triangular cell.

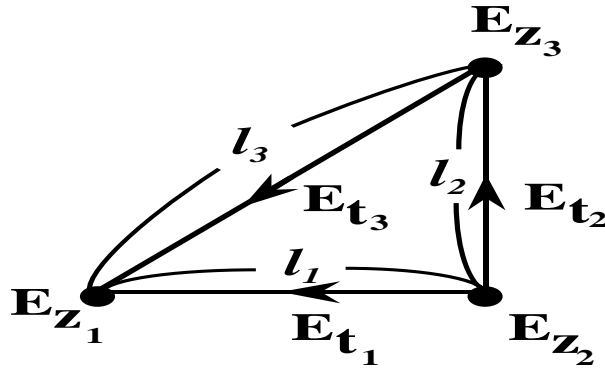


Figure 5.1: The electric field on the edges and nodes of a small triangular cell

For a small cell as shown in Figure 5.1, the electric field on the nodes is $E_{z_1}, E_{z_2}, E_{z_3}$, and the electric field on the edges is $E_{t_1}, E_{t_2}, E_{t_3}$. Because the electric field on the nodes is in the axial direction and the electric field on the edge is on the transverse plane, the shape functions for the electric field on the edges are independent from the shape functions for the electric field on the nodes. For a point (x, y) inside the small

triangular cells, the electrical field in the axial direction is represent by:

$$E_z = a + bx + cy \quad (5.1)$$

where a, b, and c are the coefficients of the linear equation. In order to simplify the mathematical calculation for the linear equations, Equation (5.1) is rewritten as the matrix form

$$E_z = [1 \ x \ y] \begin{bmatrix} a \\ b \\ c \end{bmatrix} \quad (5.2)$$

Because a, b, and c are unknown, we replace them by the field intensities on the three corner nodes of the small triangular cell and the variables of location axes for these three corner nodes. After we substitute the electric field, $E_{z_1}, E_{z_2}, E_{z_3}$, on the corner nodes, $P_1(x_1, y_1), P_2(x_2, y_2), P_3(x_3, y_3)$, into Equation (5.2), we get the matrix equation:

$$\begin{bmatrix} E_{z_1} \\ E_{z_2} \\ E_{z_3} \end{bmatrix} = \begin{bmatrix} 1 & x_1 & y_1 \\ 1 & x_2 & y_2 \\ 1 & x_3 & y_3 \end{bmatrix} \begin{bmatrix} a \\ b \\ c \end{bmatrix} \quad (5.3)$$

Solve for the coefficient a, b, and c, Equation (5.3) becomes

$$\begin{bmatrix} a \\ b \\ c \end{bmatrix} = \begin{bmatrix} 1 & x_1 & y_1 \\ 1 & x_2 & y_2 \\ 1 & x_3 & y_3 \end{bmatrix}^{-1} \begin{bmatrix} E_{z_1} \\ E_{z_2} \\ E_{z_3} \end{bmatrix} \quad (5.4)$$

In order to describe the electric field in the axial direction inside the small triangular cell in terms of E_{z_1}, E_{z_2} , and E_{z_3} , we substitute Equation (5.4) into Equation (5.2)

and get

$$E_z = [1 \ x \ y] \begin{bmatrix} 1 & x_1 & y_1 \\ 1 & x_2 & y_2 \\ 1 & x_3 & y_3 \end{bmatrix}^{-1} \begin{bmatrix} E_{z_1} \\ E_{z_2} \\ E_{z_3} \end{bmatrix} \quad (5.5)$$

After solving the inverse matrix in Equation (5.5), the electric field in the axial direction inside the small triangular cell is

$$\begin{aligned} E_z &= \frac{1}{2A_e} [1 \ x \ y] \begin{bmatrix} x_2y_3 - x_3y_2 & x_1y_3 - x_3y_1 & x_1y_2 - x_2y_1 \\ y_3 - y_2 & y_3 - y_1 & y_2 - y_1 \\ x_3 - x_2 & x_3 - x_1 & x_2 - x_1 \end{bmatrix} \begin{bmatrix} E_{z_1} \\ E_{z_2} \\ E_{z_3} \end{bmatrix} \\ &= \frac{1}{2A_e} [x_2y_3 - x_3y_2 + (y_3 - y_2)x + (x_3 - x_2)y] E_{z_1} \\ &\quad + \frac{1}{2A_e} [x_1y_3 - x_3y_1 + (y_3 - y_1)x + (x_3 - x_1)y] E_{z_2} \\ &\quad + \frac{1}{2A_e} [x_1y_2 - x_2y_1 + (y_2 - y_1)x + (x_2 - x_1)y] E_{z_3} \end{aligned} \quad (5.6)$$

where A_e is the area of the small triangular cell. From Equation (5.6), the shape functions for the electric field in the axial direction on the node elements of the small triangular cells are

$$\{N\} = \left\{ \begin{array}{l} \frac{1}{2A_e} [x_2y_3 - x_3y_2 + (y_3 - y_2)x + (x_3 - x_2)y] \\ \frac{1}{2A_e} [x_1y_3 - x_3y_1 + (y_3 - y_1)x + (x_3 - x_1)y] \\ \frac{1}{2A_e} [x_1y_2 - x_2y_1 + (y_2 - y_1)x + (x_2 - x_1)y] \end{array} \right\} \quad (5.7)$$

The partial derivatives in X direction and in Y direction for the shape functions in Equation (5.7) are

$$\{N_x\} = \left\{ \begin{array}{l} \frac{1}{2A_e} (y_3 - y_2) \\ \frac{1}{2A_e} (y_3 - y_1) \\ \frac{1}{2A_e} (y_2 - y_1) \end{array} \right\} \quad (5.8)$$

and

$$\{N_y\} = \begin{Bmatrix} \frac{1}{2A_e}(x_3 - x_2) \\ \frac{1}{2A_e}(x_3 - x_1) \\ \frac{1}{2A_e}(x_2 - x_1) \end{Bmatrix} \quad (5.9)$$

By the same token, the shape functions for the X-component field on the edge elements of the small triangular cell are

$$\{U\} = \begin{Bmatrix} \frac{1}{2A_e}l_1(y_3 - y) \\ \frac{1}{2A_e}l_2(y_1 - y) \\ \frac{1}{2A_e}l_3(y_2 - y) \end{Bmatrix} \quad (5.10)$$

where l_1 is the length of edge 1, l_2 is the length of edge 2, and l_3 is the length of edge 3 as shown in Figure 5.1. The shape functions for the Y-component field on the edge elements of the small triangular cell are

$$\{V\} = \begin{Bmatrix} \frac{1}{2A_e}l_1(x - x_3) \\ \frac{1}{2A_e}l_2(x - x_1) \\ \frac{1}{2A_e}l_3(x - x_2) \end{Bmatrix} \quad (5.11)$$

The partial derivatives in Y direction of shape functions $\{U\}$ are

$$\{U_y\} = \begin{Bmatrix} -\frac{1}{2A_e}l_1 \\ -\frac{1}{2A_e}l_2 \\ -\frac{1}{2A_e}l_3 \end{Bmatrix} \quad (5.12)$$

and the partial derivatives in X direction of shape functions $\{V\}$ are

$$\{V_x\} = \begin{Bmatrix} \frac{1}{2A_e}l_1 \\ \frac{1}{2A_e}l_2 \\ \frac{1}{2A_e}l_3 \end{Bmatrix} \quad (5.13)$$

After we substitute the shape functions, $\{U\}$, $\{V\}$, $\{N\}$, and the partial derivatives of the shape functions, $\{U_y\}$, $\{V_x\}$, $\{N_x\}$, $\{N_y\}$ into the integrals in Equation (3.13) for a small triangular cell, we get[15]

$$\begin{aligned}
\left[\iint_e \{U\} \{U\}^T dx dy \right]_{ij} &= \left[\iint_e \frac{1}{4A_e^2} l_i l_j (y_{m(i+2,3)} - y) (y_{m(j+2,3)} - y) dx dy \right]_{ij} \\
&= \frac{1}{4A_e} l_i l_j \left[y_{m(i+2,3)} y_{m(j+2,3)} - y_c (y_{m(i+2,3)} + y_{m(j+2,3)}) \right. \\
&\quad \left. + \frac{1}{12} (y_1^2 + y_2^2 + y_3^2 + 9y_c^2) \right] \quad (5.14)
\end{aligned}$$

$$\begin{aligned}
\left[\iint_e \{V\} \{V\}^T dx dy \right]_{ij} &= \left[\iint_e \frac{1}{4A_e^2} l_i l_j (x_{m(i+2,3)} - x) (x_{m(j+2,3)} - x) dx dy \right]_{ij} \\
&= \frac{1}{4A_e} l_i l_j \left[x_{m(i+2,3)} x_{m(j+2,3)} - x_c (x_{m(i+2,3)} + x_{m(j+2,3)}) \right. \\
&\quad \left. + \frac{1}{12} (x_1^2 + x_2^2 + x_3^2 + 9x_c^2) \right] \quad (5.15)
\end{aligned}$$

$$\begin{aligned}
\left[\iint_e \{U_y\} \{U_y\}^T dx dy \right]_{ij} &= \left[\iint_e \{V_x\} \{V_x\}^T dx dy \right]_{ij} \\
&= \left[\iint_e \frac{1}{4A_e^2} l_i l_j \right]_{ij} \\
&= \frac{1}{4A_e} l_i l_j \quad (5.16)
\end{aligned}$$

$$\begin{aligned}
\left[\iint_e \{U_y\} \{V_x\}^T dx dy \right]_{ij} &= \left[\iint_e \{V_x\} \{U_y\}^T dx dy \right]_{ij} \\
&= - \left[\iint_e \frac{1}{4A_e^2} l_i l_j \right]_{ij} \\
&= - \frac{1}{4A_e} l_i l_j \quad (5.17)
\end{aligned}$$

$$\begin{aligned}
\left[\iint_e \{U\} \{N_x\}^T dx dy \right]_{ij} &= \left[\iint_e \frac{1}{4A_e^2} l_i (y_{m(j+2,3)} - y_{m(j+1,3)}) (y_{m(i+2,3)} - y) dx dy \right]_{ij} \\
&= \frac{1}{4A_e} l_i (y_{m(j+1,3)} - y_{m(j+2,3)}) (y_{m(i+2,3)} - y_c) \quad (5.18)
\end{aligned}$$

$$\begin{aligned}
\left[\iint_e \{V\} \{N_y\}^T dx dy \right]_{ij} &= \left[\iint_e \frac{1}{4A_e^2} l_i (x_{m(j+2,3)} - x_{m(j+1,3)}) (x - x_{m(i+2,3)}) dx dy \right]_{ij} \\
&= \frac{1}{4A_e} l_i (x_{m(j+1,3)} - x_{m(j+2,3)}) (x_c - x_{m(i+2,3)}) \quad (5.19)
\end{aligned}$$

$$\left[\iint_e \{N\} \{N\}^T dx dy \right]_{ij} = \begin{cases} \frac{A_e}{6}, & \text{for } i=j \\ \frac{A_e}{12}, & \text{for } i \neq j \end{cases} \quad (5.20)$$

$$\begin{aligned}
&\left[\iint_e \{N_x\} \{N_x\}^T dx dy \right]_{ij} \\
&= \left[\iint_e \frac{1}{4A_e^2} (y_{m(i+2,3)} - y_{m(i+1,3)}) (y_{m(j+2,3)} - y_{m(j+1,3)}) \right]_{ij} dx dy \\
&= \frac{1}{4A_e} (y_{m(i+2,3)} - y_{m(i+1,3)}) (y_{m(j+2,3)} - y_{m(j+1,3)}) \quad (5.21)
\end{aligned}$$

$$\begin{aligned}
&\left[\iint_e \{N_y\} \{N_y\}^T dx dy \right]_{ij} \\
&= \left[\iint_e \frac{1}{4A_e^2} (x_{m(i+2,3)} - x_{m(i+1,3)}) (x_{m(j+2,3)} - x_{m(j+1,3)}) \right]_{ij} dx dy \\
&= \frac{1}{4A_e} (x_{m(i+2,3)} - x_{m(i+1,3)}) (x_{m(j+2,3)} - x_{m(j+1,3)}) \quad (5.22)
\end{aligned}$$

with

$$x_c = \frac{x_1 + x_2 + x_3}{3} \quad (5.23)$$

$$y_c = \frac{y_1 + y_2 + y_3}{3} \quad (5.24)$$

$$m(i, k) = \text{mod}(i - 1, k) + 1 \quad (5.25)$$

where the subscripts i, j are used to indicate the component at i row and j column in the matrix, and $\text{mod}(i, k)$ equals to the remainder of $(\frac{i}{k})$.

The matrices in Equations (3.15) to (3.18) are the summation of the shape functions and the derivatives of the shape functions of the elements for all the small triangular cells. With Equations (5.14) to (5.22), we substitute the integrated results into the elements in Equations (3.15) to (3.18) for all the small triangular cells, then the eigenvalue equation is constructed.

5.2 Vector MEI Boundary Condition for the Elements in the Axial Direction

The boundary condition for the axial elements is to determine the field intensities of the elements on the artificial boundary by the MEI boundary equations instead of the hybrid edge/nodal VFEM mesh equations. In order to truncate the infinite open space, the MEI boundary equations are used to replace the node elements on the boundary in the axial direction in Equation (3.20), and we get

$$\gamma [K'_{zt}] \{E_t\} - [K'_{zz}] \{E_z\} = \{0\}. \quad (5.26)$$

The i th row of matrix $[K'_{zt}]$ and $[K'_{zz}]$ in Equation (5.26) contain the coefficients of a linear equation for deciding the electric field distribution of the i th element. In order to make the boundary elements in Equation (5.26) become independent of the propagation constant, the rows of the boundary elements in the axial direction are assigned to zeros for matrix $[K'_{zt}]$. The rows of the boundary elements in the axial direction are replaced by the finite difference equations from the MEI boundary condition for matrix $[K'_{zz}]$. The electric field distribution on the boundary nodes is, therefore, determined by the finite difference equations which are calculated for truncating the infinite space by an artificial boundary – MEI boundary condition.

5.3 Vector MEI Boundary Condition for the Elements in Transverse Direction

In order to truncate the open space for the hybrid edge/nodal VFEM calculation, we apply the MEI boundary condition for the edge elements on the boundary in Equation (3.21) and get

$$[K'_{tt}] \{E_t\} - \gamma^2 \left([K_{tz}] [K_{zz}]^{-1} [K_{zt}] + [M_{tt}] \right)' \{E_t\} = 0. \quad (5.27)$$

We call matrix equation (5.27) HTMEI equation with HTMEI standing for Hybrid edge/nodal FEM with the Three-component MEI Boundary Condition. The rows of the boundary elements in matrix $\left([K_{tz}] [K_{zz}]^{-1} [K_{zt}] + [M_{tt}] \right)'$ of Equation (5.27) are assigned to zeros for making the boundary condition independent of the propagation constant, γ . The rows of the boundary elements in matrix $[K_{tt}]$ are replaced by the finite difference equations from the MEI boundary condition. By solving the eigenvalues of Equation (5.27) as described in Chapter 3, we can get the propagation constants for different propagation modes of the transmission line.

Chapter 6

Transmission Loss and Electric Current Distribution in the Conductor

In order to estimate the transmission loss and the electric field distribution in the conductor more accurately, the hybrid edge/nodal VFEM with the 3-component MEI boundary condition is used to calculate the electric field distribution on the cross section of the transmission line. The boundary condition truncates the infinite space by a layer of boundary elements. The calculated results by using edge/nodal VFEM with the 3-component MEI boundary condition are close to the measured data at the frequencies below 1 GHz. At high frequency (> 1 GHz), the conduction current density concentrates in the area close to the conductor surface due to skin effect. Because the surface roughness of the conductor and the transmission loss from the ground are not included in the calculation, the measured data are higher than the calculated results at high frequency. The calculated results can be used to choose the best structure for the transmission line to be used in the MCM without the cost of making samples, and for reducing the turn around time for improving performance.

6.1 The Triplate Strip Line

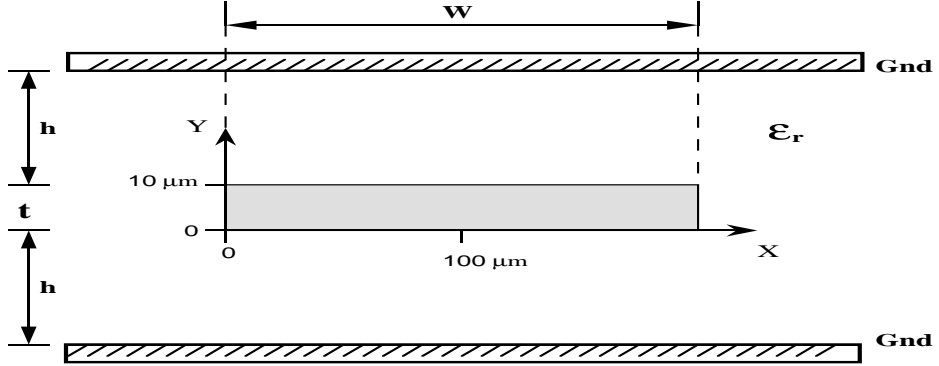


Figure 6.1: The cross section of a triplate line

The hybrid edge/nodal VFEM with the 3-component MEI boundary condition is used to calculate the transmission loss of a triplate strip. The cross section of the line is illustrated in Figure 6.1. In order to compare the calculation results with the experimental data published by Taguchi et al.[34], the distance between two grounds, $2h + t$, is set to be $910\mu\text{m}$, the thickness of the conducting strip, t , $10\mu\text{m}$, and the width of the strip, w , $200\mu\text{m}$. For the dielectric, the relative dielectric constant, ϵ_r , is set to be 7.55, and the loss tangent, $\tan \delta$, is 0.005. The conductivity, σ , of the copper (Reduction from CuO) is $2.5 \times 10^7 \text{S/m}$ [34]. The structure parameters of triplate strip line are summarized in Table 6.1.

The transmission loss is a function of frequency as shown in Figure 6.2. The theoretical values are simulated by HP85150 Microwave Design System (MDS). The results calculated by the hybrid edge/nodal VFEM with the 3-component MEI boundary condition are close to the theoretical values which do not include the loss from

Table 6.1: The structure parameters for the triplate transmission line

| | | |
|------------------------------------|-------------------|-------------------|
| Width of the strip | 200 | (μm) |
| Thickness of the strip | 10 | (μm) |
| Height of the strip | 450 | (μm) |
| Distance between two ground plates | 910 | (μm) |
| Conductivity of the strip | 2.5×10^7 | (S/m) |
| Relative dielectric constant | 7.55 | |
| Loss tangent of dielectric | 0.005 | |

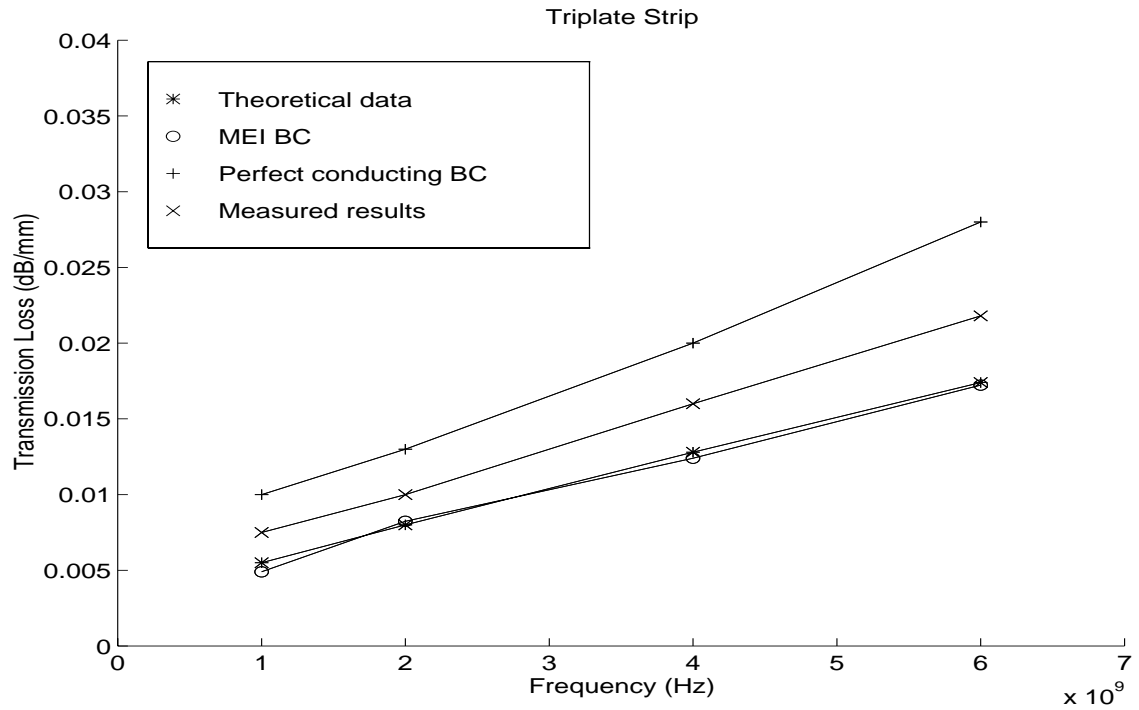


Figure 6.2: Calculated and measured transmission loss vs frequency

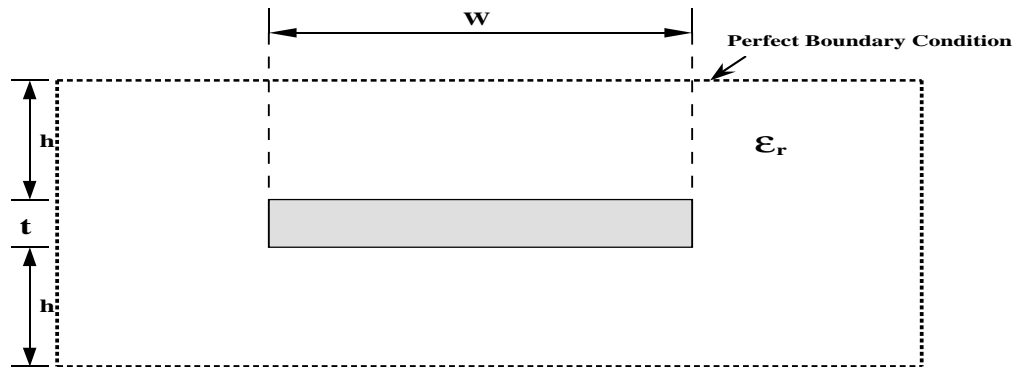


Figure 6.3: The perfect conductor boundary condition on the cross section of the triplate line

the ground, but the results calculated by the edge/nodal VFEM with a wall of perfect conductor[3] as its boundary condition are larger than the theoretical results and measured data. The perfect conductor boundary condition used in [3] is shown in Figure 6.3. The measured data are higher than our calculated results, because our calculated results do not include the loss from ground plane. The 3-component MEI boundary condition makes the field distribution in the dielectric close to the real situation, and improves the accuracy of the calculation.

In order to know how the current density distribution on the cross section of the conductor affects the transmission loss, we plot the current density distributions on the cross section of the conductor for different frequencies. For 2 GHz, 4 GHz, and 6 GHz, the current density distributions in the strip conductor are shown in Figure 6.4, Figure 6.5, and Figure 6.6. At high frequency, the current density distribution concentrates on the area close to the conductor surface, and the effective cross-section area for conduction current is smaller than the effective cross-section area at low frequency. Therefore, the transmission loss is larger for higher frequency

wave propagation.

The Current Density

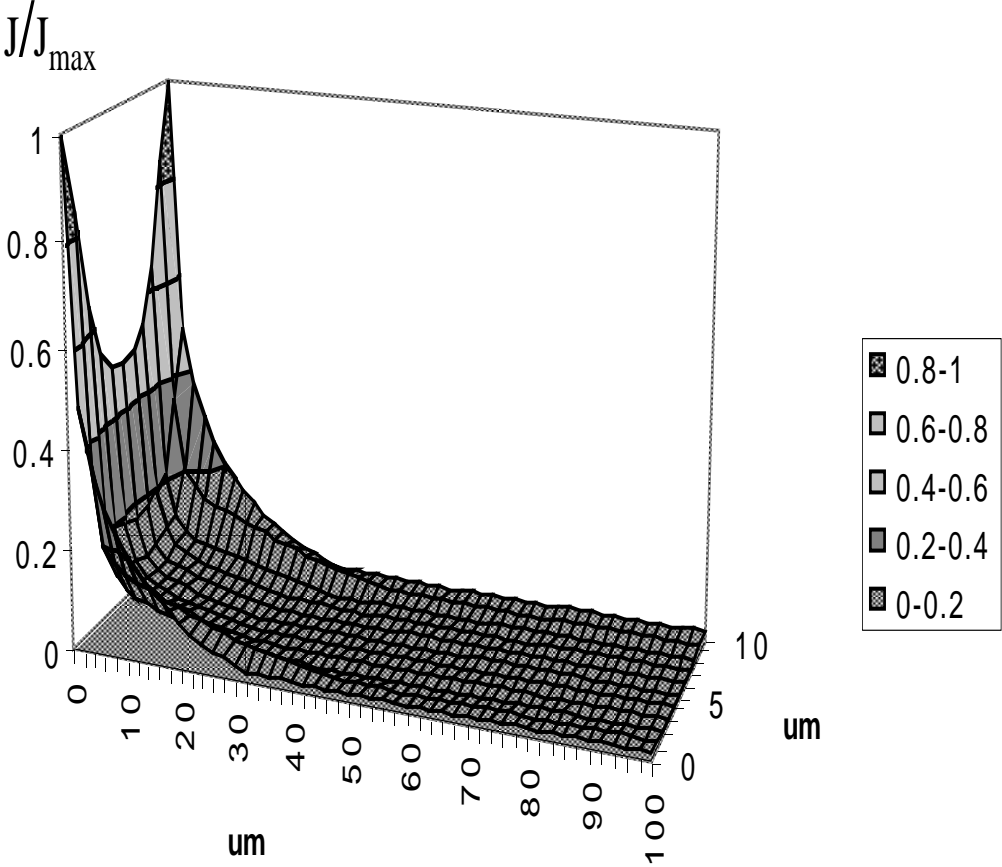


Figure 6.4: The current density distribution on the cross section of the center strip of the triplate geometry at 2 GHz

The Current Density

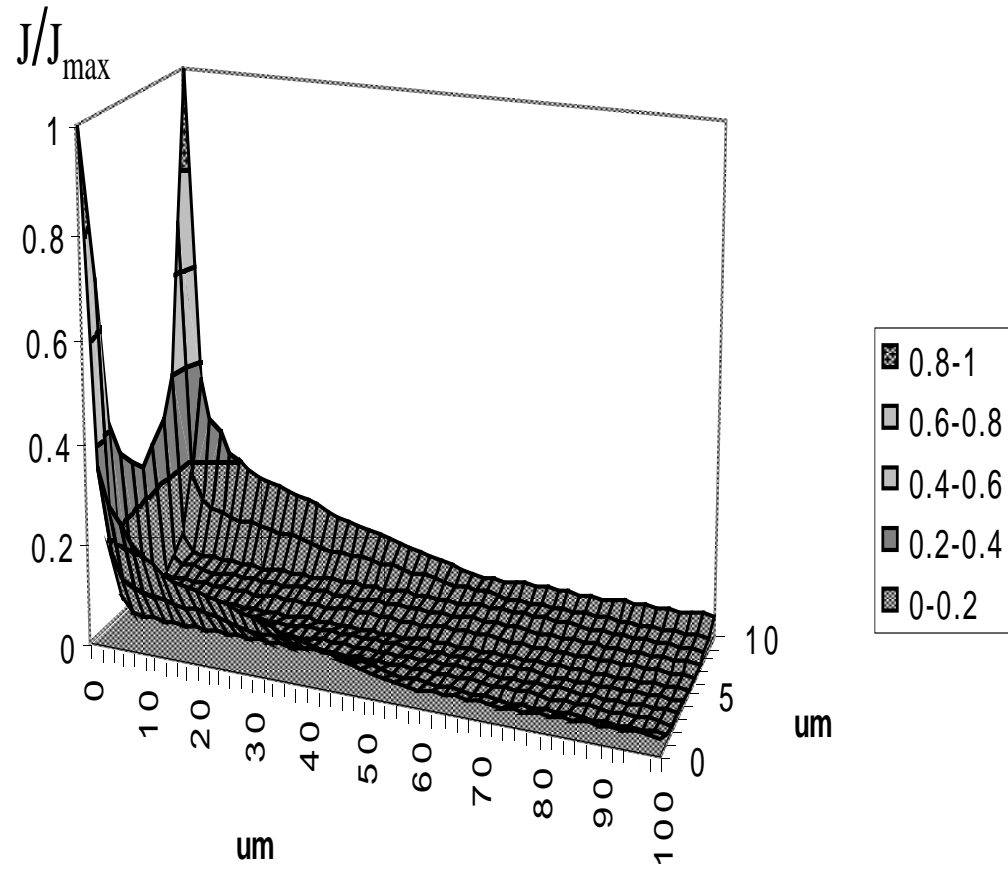


Figure 6.5: The current density distribution on the cross section of the center strip of the triplate geometry at 4 GHz

The Current Density

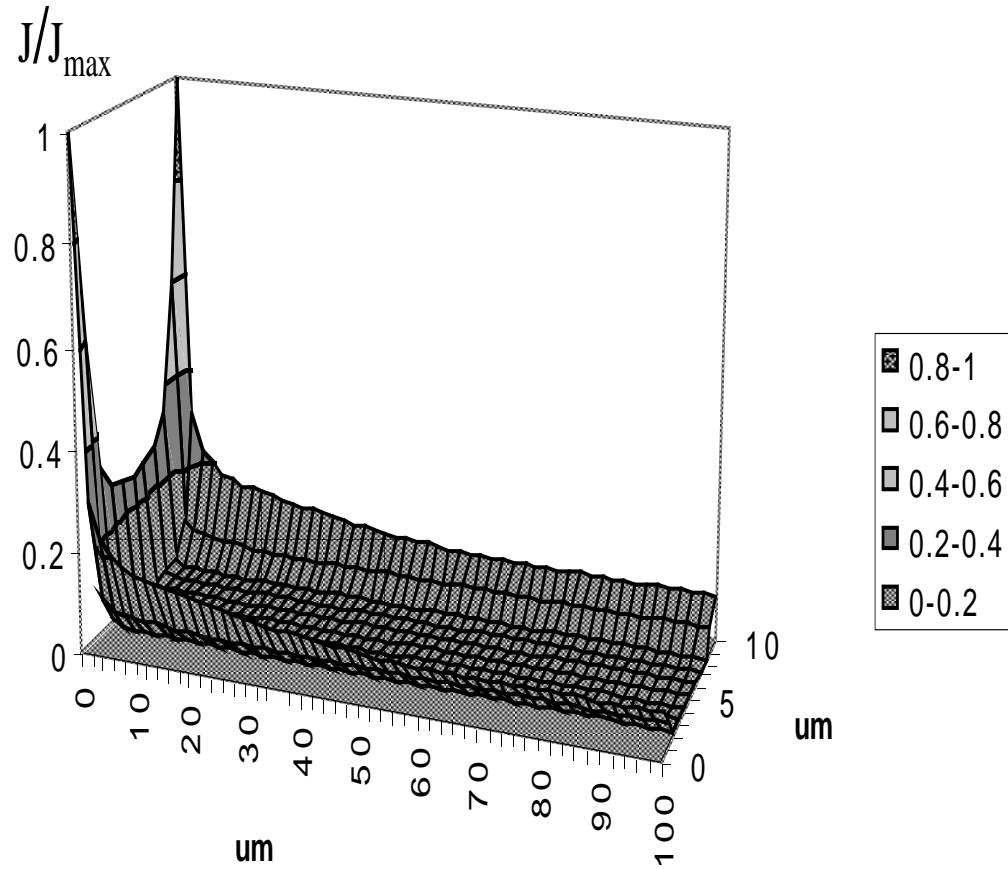


Figure 6.6: The current density distribution on the cross section of the center strip of the triplate geometry at 6 GHz

6.2 The Transmission Line in an MCM

There are several technologies of MCM manufacturing which vary in the dimensions of the transmission line structure and the materials used. We compare our calculation results with the measured data for the interconnection in an MCM manufactured by Silicon Graphic Incorporated (SGI). The cross section of the transmission line in the MCM is shown in Figure 6.7.

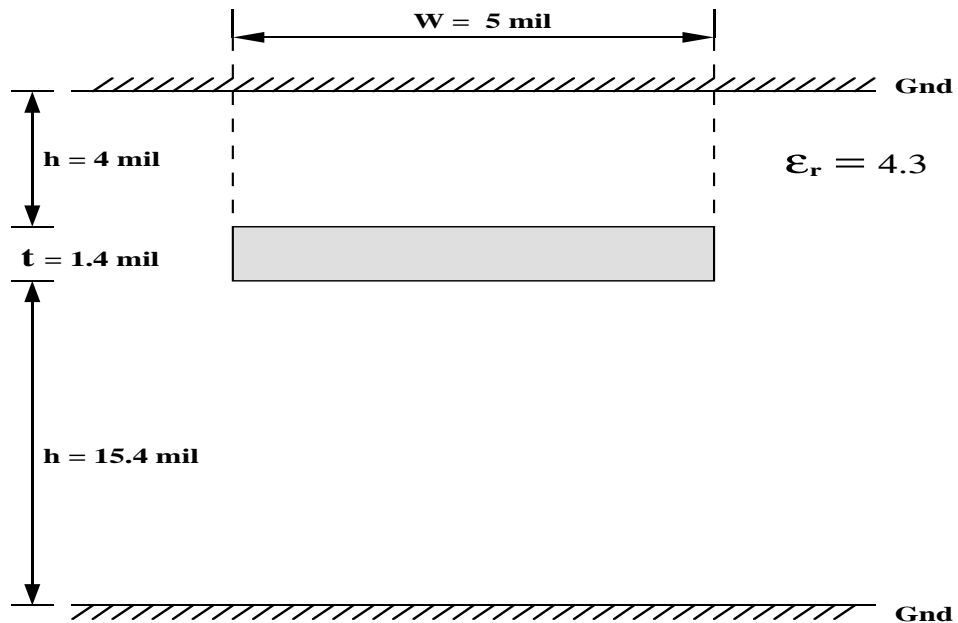


Figure 6.7: The cross section of a transmission line in a MCM

The width of the conductor is 5 mil, and the thickness of the conductor is 1.4 mil. The height of the conductor is 15.4 mil, and the distance between the two grounds is 20.8 mil. The dielectric is lossless, and the relative dielectric constant is 4.3. The conductor is copper with conductivity $5.7 \times 10^7 \text{ S/m}$. The structure parameters of the

transmission line in an MCM manufactured by SGI are summarized in Table 6.2.

Table 6.2: The structure parameters for the transmission line in an MCM manufactured by SGI

| | | |
|------------------------------------|-------------------|-------|
| Width of the strip | 5 | (mil) |
| Thickness of the strip | 1.4 | (mil) |
| Height of the strip | 15.4 | (mil) |
| Distance between two ground plates | 20.8 | (mil) |
| Conductivity of the strip | 5.7×10^7 | (S/m) |
| Relative dielectric constant | 4.3 | |
| Loss tangent of dielectric | 0.00 | |

We calculate the transmission loss by using the hybrid edge/nodal FEM with the 3-component MEI boundary condition and compare the calculated results with the measured data. The calculated results are almost the same as the measured data except for the transmission loss at high frequency as shown in Figure 6.8. As the wave frequency goes higher (close to one GHz), the calculated results is smaller than the measured data. The numerical calculation is based on the assumption that the ground is lossless; therefore, the calculated transmission loss should be smaller than the measured data at high frequency. The transmission loss from the ground will also increase as the frequency increases.

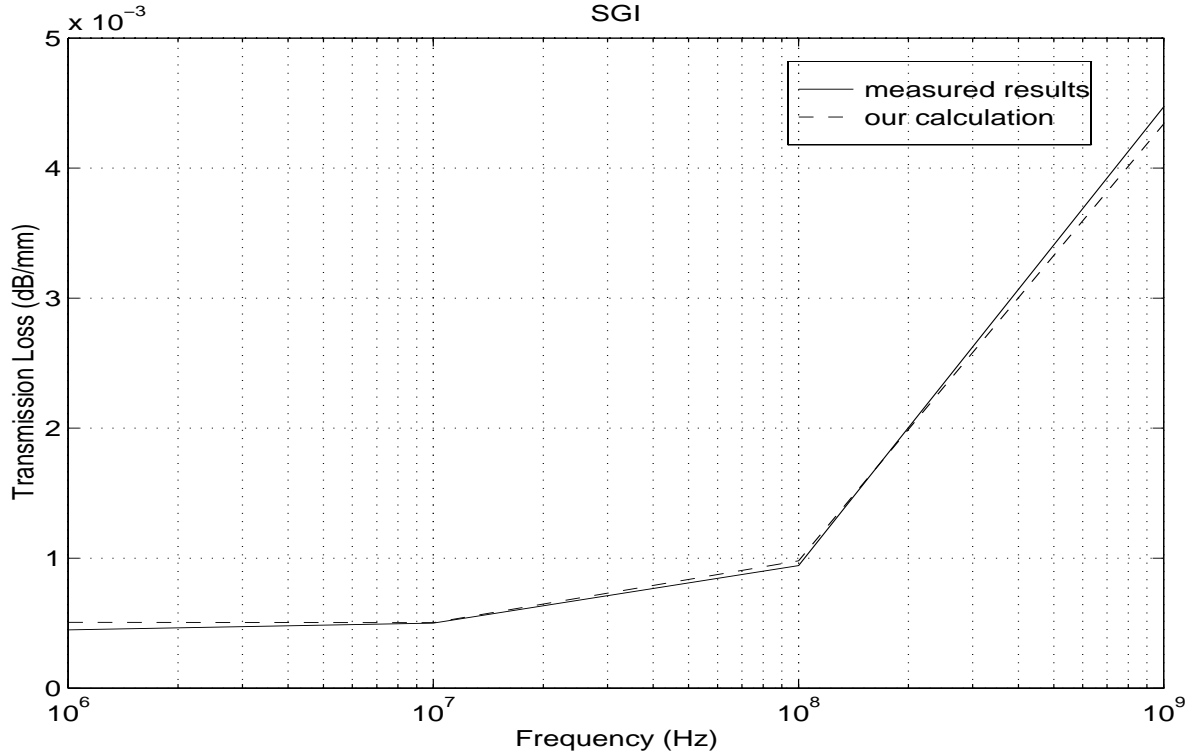


Figure 6.8: The transmission loss vs frequency for the transmission line in an MCM

6.3 The Coated Interconnection Used in an MCM

The MCM manufacturers usually use copper as the conducting metal due to its low resistivity which provides the MCM technologies a distinct performance advantage at low cost. Polyimide is chosen as the dielectric material in the MCM package for its low dielectric loss. In order to eliminate the reaction between copper and polyimide[2, 16], a diffusion barrier layer between copper and polyimide is often added by the manufacturers. There are two barrier layers reported[1]: a thin film of inorganic dielectric and a thin film of metal. We used the structures published by Adema et al.[1] to calculate the propagation losses of the microstrip transmission lines and

compare the calculated results with the measured data. The structures in Adema et al.[1] are: the microstrip clad with inorganic dielectric and the microstrip coated with chromium.

6.3.1 The Microstrip Clad with Inorganic Dielectric

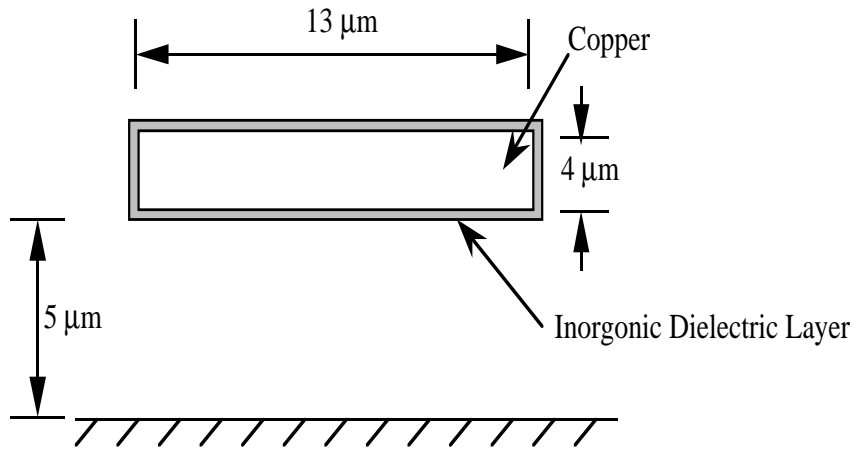


Figure 6.9: The transmission line with a thin-film inorganic dielectric.

For the microstrip structure shown in Figure 6.9, the strip conductor is buried in the polyimide dielectric with a ground plane under it and the space above strip conductor is filled with polyimide. The strip conductor is copper clad with a thin film of inorganic dielectric. The dimensions of the structure are shown in Figure 6.9. The thickness of the thin-film inorganic dielectric is much smaller than the thickness of the conductor. Because the transmission loss from the strip conductor is much larger than the loss from the inorganic dielectric, the electric properties of the inorganic dielectric are assumed the same as the electronic properties of polyimide to simplify the numerical calculation. The loss tangent of inorganic dielectric is assumed to be

zero, and the relative dielectric constant, ϵ_r , is 3.0, which is the same as the relative dielectric constant of polyimide for the transmission loss calculation. The conductivity of copper for the strip conductor is $5.8 \times 10^7 \text{ S/m}$. The structure parameters of the clad microstrip conductor are summarized in Table 6.3.

Table 6.3: The structure parameters for the clad microstrip

| | | |
|------------------------------|-------------------|-------------------|
| Width of the strip | 13 | (μm) |
| Thickness of the strip | 4 | (μm) |
| Height of the strip | 5 | (μm) |
| Conductivity of the strip | 5.8×10^7 | (S/m) |
| Relative dielectric constant | 3.0 | |
| Loss tangent of dielectric | 0.00 | |

The transmission loss of the inorganic dielectric clad microstrip is a function of frequency as shown in Figure 6.10. The calculated transmission loss is smaller than the measured data because the transmission loss from the ground and the cladding dielectric is not included for the numerical calculation. At low frequency, the skin depth of the conductor is larger than the thickness of the conductor, the major transmission loss comes from the strip conductor. Therefore, the difference of the transmission loss between the calculated results and the measured data is smaller at a lower wave frequency.

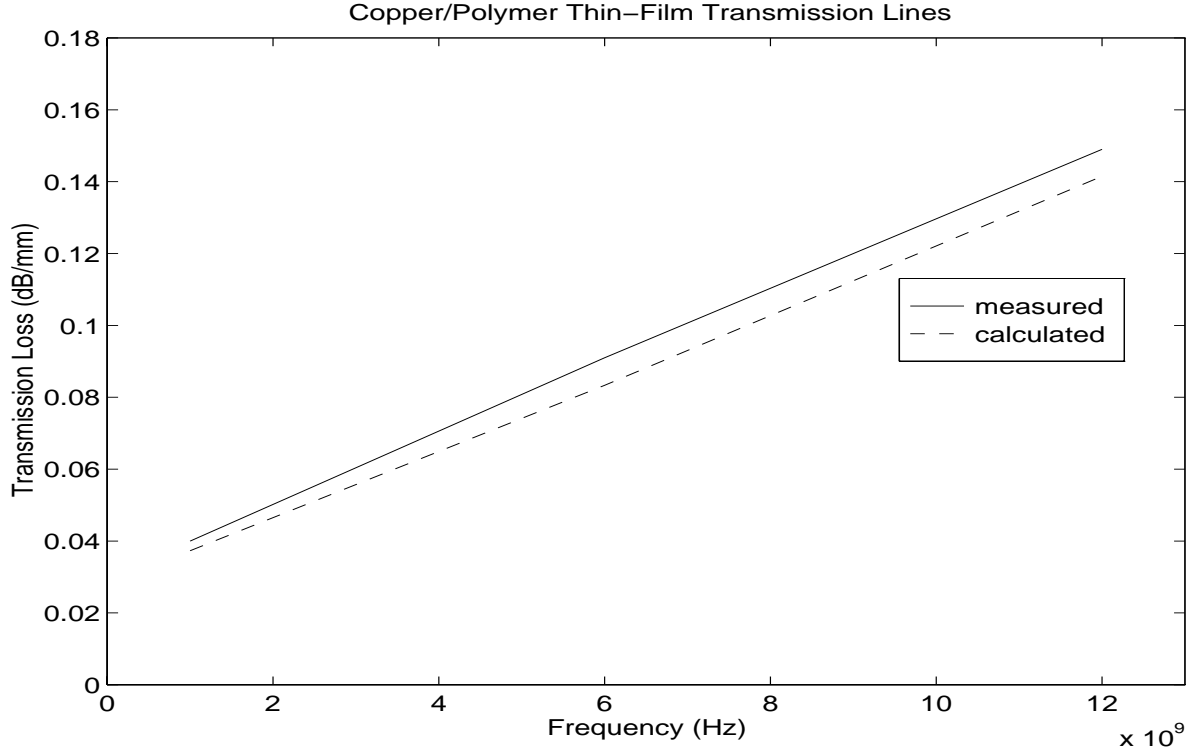


Figure 6.10: The transmission loss vs frequency for the microstrip coated with a thin-film inorganic

6.3.2 The Microstrip Coated with Chromium

By using a Balzers BAK 760 electron-beam evaporator[1], the strip conductor is constructed of Cr/Cu/Cr with the thickness of $100\text{\AA}/4\mu\text{m}/100\text{\AA}$ as shown in Figure 6.11. The thickness and width of the copper conductor in Figure 6.11 are the same as the copper conductor in Figure 6.9 for comparing the transmission loss between these two microstrips. The conductivity of the copper is $5.8 \times 10^7\text{S/m}$, but the conductivity of chromium is only $7.75 \times 10^6\text{S/m}$. The structure parameters of the microstrip conductor coated with chromium are summarized in Table 6.4.

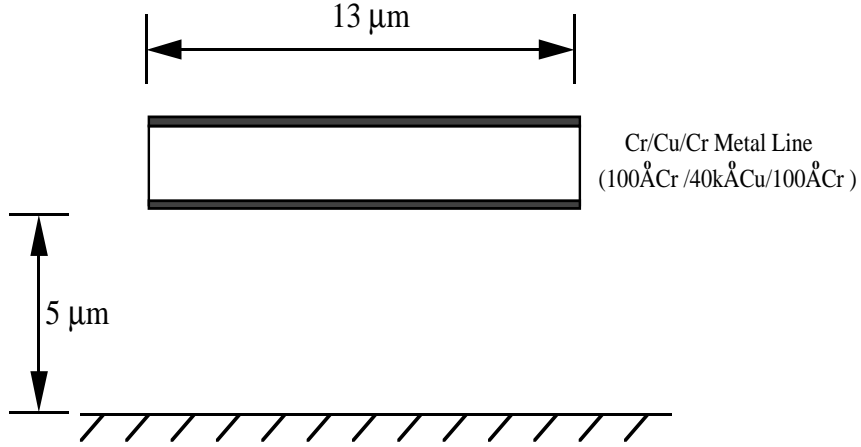


Figure 6.11: The transmission line coated with a thin-film chromium.

Table 6.4: The structure parameters for the Chromium coated microstrip

| | | |
|------------------------------|--------------------|-------------------|
| Width of the strip | 13 | (μm) |
| Thickness of the strip | 4 | (μm) |
| Height of the strip | 5 | (μm) |
| Thickness of chromium layer | 100 | (Å) |
| Conductivity of the copper | 5.8×10^7 | (S/m) |
| Conductivity of the chromium | 7.75×10^6 | (S/m) |
| Relative dielectric constant | 3.0 | |
| Loss tangent of dielectric | 0.00 | |

As shown in Figure 6.12, the calculated transmission loss is still lower than the measured data, and the difference between the calculated results and the measured data in Figure 6.12 is smaller than the difference in Figure 6.10. That's because the loss tangent of the clad inorganic dielectric in Figure 6.9 is larger than the loss tangent of polyimide.

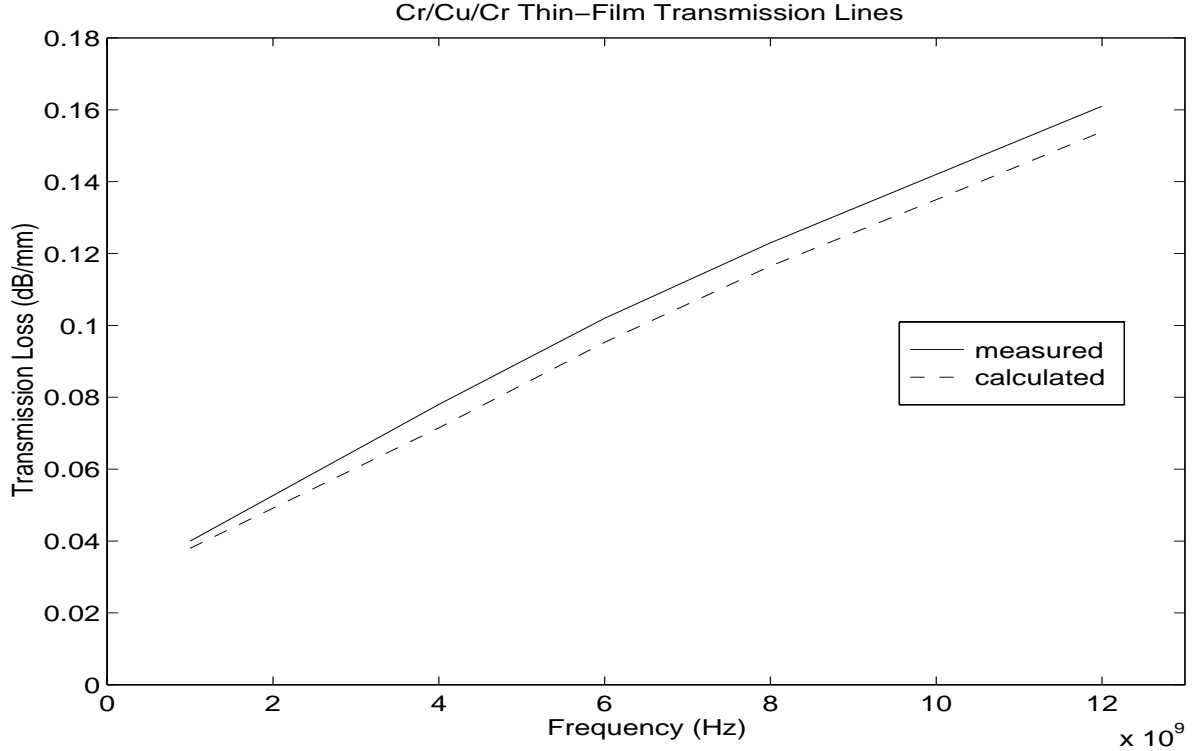


Figure 6.12: The transmission loss of a transmission line coated with chromium.

In order to choose the best transmission line structure for the system performance, we compare Figure 6.12 with Figure 6.10. The skin effect is not significant on the cross section of the conductor at low frequency, the difference between the transmission loss of the Cr/Cu/Cr microstrip and the transmission loss of the inorganic dielectric clad microstrip is small. As the frequency increases, the current density is higher in the area close to the bottom of the strip conductor. Because the resistivity of chromium is higher than the resistivity of copper, the transmission loss of the Cr/Cu/Cr microstrip is higher than the transmission loss of the inorganic dielectric clad microstrip for wave propagation at high frequency.

Chapter 7

Summary and Future Directions

In this chapter, we summarize the modeling for calculating the electromagnetic field distribution, discuss the calculated results of the field distribution, and suggest future research topics.

7.1 Summary

In this dissertation, we developed the 3-component MEI boundary condition for the hybrid edge/nodal VFEM. This 3-component MEI boundary condition is applied to the matrix equation (3.21) formed by the 3-dimensional vector Helmholtz's equation in the transmission line, then a HTMEI (Equation 5.27) is formulated. By calculating the eigenvector of the lowest-mode eigenvalue of the HTMEI equation, we obtained the field distribution on the transverse plane. The square roots of the eigenvalues are the complex propagation constants. The real part of the propagation constant is the attenuation constant and the relation between the transmission loss and attenuation constant is shown in Equation (3.9). The excitation source for generating the

propagating wave is assumed far away from the calculated area.

The boundary condition for the hybrid edge/nodal FEM is an approximate method for the field distribution calculation. The approximation is due to the limited computer resources. The infinite space with the effect of the ground plate(s) is truncated by the 3-component MEI cells for the boundary condition. The boundary condition is not only used to simulate the wave propagation in the open area, but also applied to hybrid edge/nodal FEM to calculate all the possible propagation modes. The finite difference equation of the MEI boundary condition is used to define the boundary elements for the calculation.

The transmission loss consists of the loss from the strip conductor, the loss from the dielectric, the loss from the conductor surface roughness, and the loss from the ground. The calculated transmission loss of this dissertation includes the loss from the strip conductor and the loss from the dielectric. The trend of the calculated transmission loss is consistent with the trend of the measured transmission loss. The calculated transmission loss is 5% to 10% less than the measured transmission loss in general. The relatively small difference between the calculated and measured transmission losses suggests that the transmission loss is dominated by the loss from the strip conductor, and the loss from the dielectric.

7.2 Discussion of Calculated Results

In this study, the transmission loss is derived from the attenuation constant. The attenuation constant is the real part of the complex propagation constant, which is the square root of the lowest-mode eigenvalue of the HTMEI equation. The HTMEI

equation is constructed by using the hybrid edge/nodal FEM with the 3-component MEI boundary condition. Since the 3-component MEI boundary condition is calculated by using perfect conductor as the ground plane(s), the calculated transmission loss obtained by solving the HTMEI equation does not include the transmission loss from the ground plate(s).

As the frequency increases, the transmission loss from the ground increases too. If the frequency is higher than 20 GHz, the transmission loss from the ground should be included in the calculation. The induced current density distribution in the lossy ground must be obtained in order to calculate the transmission loss from the ground. Using quasi-static assumption, we can calculate the current density distribution by the Method of Moment with the propagation current in the strip conductor as the current source. After the current density distribution in both the strip conductor and in the ground have been calculated, we can calculate the per-length resistance and per-length inductance. The per-length capacitance can be calculated by using a quasi-static assumption since the transverse current density is much smaller than the current density in axial direction inside the conductor. With the lossy ground, the complex propagation constant of the transmission line is

$$\gamma = \sqrt{(R + j\omega L)(G + j\omega C)} \quad (7.1)$$

where R , L , G , and C denotes the per-length resistance, inductance, conductance, and capacitance respectively. The per-length conductance is proportional to the loss tangent of the dielectric, and it's very small compared to $j\omega C$ for the dielectric used in MCMs.

7.3 Future Research

In this research, we applied the 3-component MEI boundary condition to the hybrid edge/nodal FEM. The calculated results are better than the hybrid edge/nodal FEM with a perfect conductor as its boundary condition (see Figure 6.3). Possible extensions are as follows:

1. Calculate the current density distribution in the lossy ground — By using quasi-static assumption and the Method of Moments with the current density distribution in the strip conductor as the current source, we can calculate the induced current density distribution in the ground by

$$\begin{aligned} -\nabla V &= j\omega\vec{A} + \rho\vec{J} \\ &= 0 \end{aligned} \tag{7.2}$$

and

$$\vec{A} = \frac{\mu}{4\pi} \int_V \frac{\vec{J}e^{-jkR}}{R} dv \tag{7.3}$$

where ρ is the resistivity of the ground, \vec{J} is the current density distribution in the conductor, k is the wave number, and \vec{A} is the vector potential induced from the current density distribution in the conductor. If the dimension of the transmission-line cross section is much smaller than the wavelength, the conduction current in the transmission line and ground far away from the calculated cross section can be neglected due to the effect of the ground. The distance are measured in term of wavelength. Equation (7.3) can be approximated[37] by

$$\vec{A} = \frac{\mu}{4\pi} \int_V \frac{\vec{J}}{R} dv \tag{7.4}$$

After we substitute Equation (7.4) into Equation (7.2) and solve it by the Method of Moments, the current density distribution in ground can be calculated.

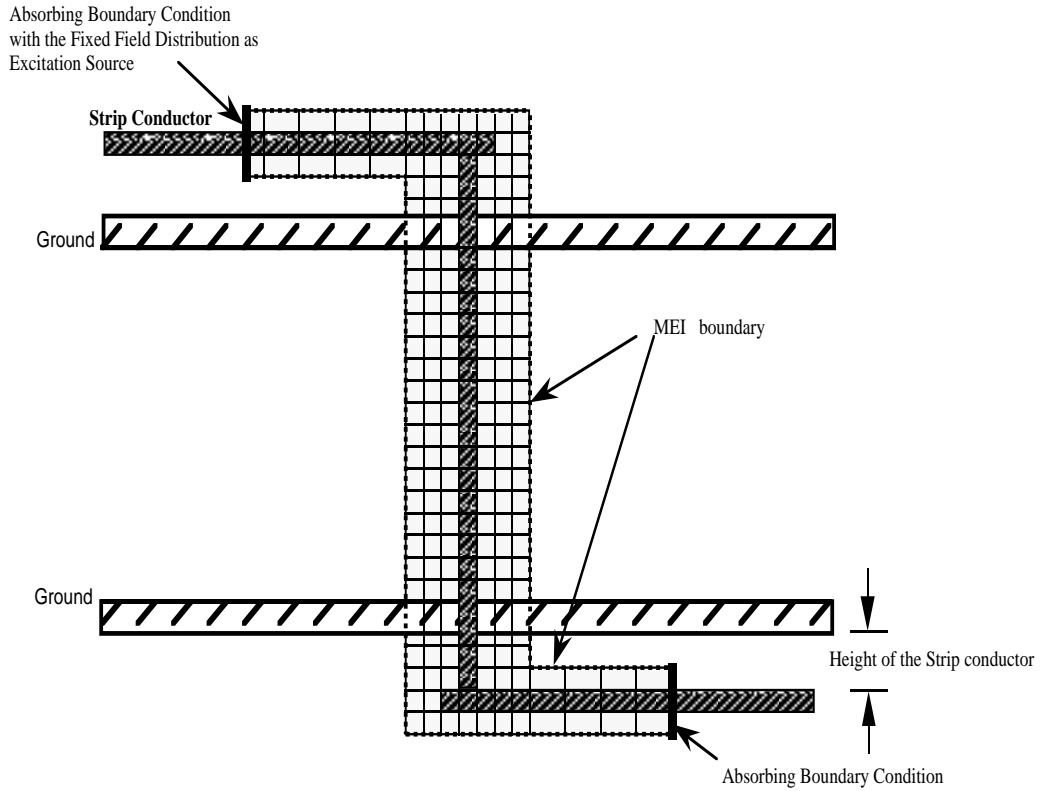


Figure 7.1: A discontinuity connecting two transmission lines

2. Use the field distribution on the cross section of the transmission line as the boundary condition on one end of a discontinuity to calculate the field distribution in the vicinity of the discontinuity — For a discontinuity connecting two transmission lines, the field distribution on the cross section of an infinite transmission line can be used as an excitation source to calculate the

scattered field distribution in the vicinity of the discontinuity. The artificial boundary other than the cross section of the transmission line is covered by the 3-component MEI boundary condition as shown in Figure 7.1. The cross section of the transmission line on two ends of the discontinuity are covered by absorbing boundary condition. Since the higher order modes of the scattered wave will decay to zero after certain distance, the distance between the absorbing boundary condition and the discontinuity needs to be at least 5 times the height of the strip conductor[35] in order to get an accurate field distribution in the vicinity of the discontinuity.

3. Modify the Green's function with the effect of the lossy ground to calculate the 3-component MEI boundary condition — If the thickness of the ground plate is much larger than the skin depth in ground, we can use the Green's function with the effect of the loss ground[10] to calculate the 3-component MEI boundary condition. The complex propagation constants calculated by the hybrid edge/nodal VFEM with the new 3-component MEI boundary condition are the propagation constant for the lossy transmission line with lossy ground. Therefore, the calculated transmission loss will include also the loss from the ground.

Bibliography

- [1] G.M. Adema, L. Hwang, and G.A. Rinne. Passivation schemes for copper/polymer thin-film interconnections used in multichip modules. *IEEE Transactions on Components, Hybrids, and Manufacturing Technology*, 16:53–59, February 1993.
- [2] G.M. Adema, I. Turlik, L. Hwang, G.A. Rinne, and M.J. Berry. Effects of polymer/metal interaction in thin-film multichip module applications. *IEEE Transactions on Components, Hybrids, and Manufacturing Technology*, 13:766–774, December 1990.
- [3] M.S. Alam, M. Koshiba, K. Hirayama, and Y. Hayashi. Analysis of lossy planar transmission lines by using a vector finite element method. *IEEE Transactions on Microwave Theory and Techniques*, 43:2466–2471, October 1995.
- [4] C.J. Bartlett, J.M. Segelken, and N.A. Teneketges. Multichip packaging design for VLSI-base system. *IEEE Transactions on Components, Hybrids, and Manufacturing Technology*, 4:647–653, December 1987.
- [5] J.R. Brews. Transmission line models for lossy waveguide interconnections in vlsi. *IEEE Transactions on Electron Devices*, 9, September 1986.

- [6] A.C. Cangellaris, J.L. Prince, and O.A. Palusinski. Real inductance calculation for high-speed interconnect system. *International Electronics Packaging Society*, pages 596–600, 1988.
- [7] A.C. Cangellaris, J.L. Prince, and L. Vakanas. Frequency-dependent inductance and resistance calculation for a three-dimensional structures in high-speed interconnection systems. *Proceedings of Electronic Components Conference*, pages i398–403, 1989.
- [8] A.C. Cangellaris and D.B. Wright. Application of the measured equation of invariance to electromagnetic scattering by penetrable bodies. *IEEE Transactions on Magnetics*, 29:1628–1631, March 1993.
- [9] E.J. Denlinger. A frequency dependent solution for microstrip transmission lines. *IEEE Transactions on Microwave Theory and Techniques*, 1:30–39, January 1971.
- [10] R. Faraji-Dana and Y.L. Chow. The current distribution and ac resistance of a microstrip structure. *IEEE Transactions on Microwave Theory and Techniques*, 38:1268–1277, September 1990.
- [11] H.E. Green. The numerical solution of some important transmission line problems. *IEEE Transactions on Microwave Theory and Techniques*, 13:676–692, September 1965.
- [12] R. F. Harrington. *Time-harmonic electromagnetic fields*. McGraw-Hill, 1961.
- [13] S. Koike, N. Yoshida, and I. Fukai. Transient analysis of coupling between crossing lines in three-dimensional space. *IEEE Transactions on Microwave Theory*

- and Techniques*, 35:67–71, January 1987.
- [14] M. Koshiba and K. Inoue. Simple and efficient finite-element analysis of microwave and optical waveguides. *IEEE Transactions on Microwave Theory and Techniques*, 40:371–377, February 1992.
- [15] M. Koshiba, S. Maruyama, and K. Hirayama. A vector finite element method with the high-order mixed-interpolation-type triangular elements for optical waveguiding problems. *IEEE Transactions on Microwave Theory and Techniques*, 12:495–502, March 1994.
- [16] S.P. Kowalczyk, Y.H. Kim, G.F. Walker, and J. Kim. Polyimide on copper: The role of solvent in the formation of copper precipitates. *Appl. Phys. Lett*, 52:375–376, February 1988.
- [17] J.-F. Lee, D.-K. Sun, and Z.J. Cendes. Full-wave analysis of dielectric waveguides using tangential vector finite elements. *IEEE Transactions on Microwave Theory and Techniques*, 39:1262–1271, August 1991.
- [18] G. Liang, Y. Liu, and K.K. Mei. Full-wave analysis of coplanar waveguide and slotline using the time-domain finite-difference method. *IEEE Transactions on Microwave Theory and Techniques*, 37:1949–1957, December 1989.
- [19] B.H. McDonald and A. Wexler. Finite element solution of unbounded field problems. *IEEE Transactions on Microwave Theory and Techniques*, 20:841–847, December 1972.
- [20] K. Mei, R. Pous, Z. Chen, Y. Liu, and M. Prouty. Measured equation of invariance: A new concept in field computation. *IEEE Transactions on Antennas and*

- Propagations*, 42:320–327, March 1994.
- [21] K.K. Mei and J.G. Van Bladel. Scattering by perfect-conducting rectangular cylinders. *IEEE Transactions on Antennas and Propagations*, pages 185–192, March 1963.
- [22] K.K. Mei and J Fang. Superabsorption – a method to improve absorbing boundary condition. *IEEE Transactions on Antennas and Propagations*, 9:1001–1010, September 1992.
- [23] K.K. Mei and Y. Liu. Comments on “a theory and numerical analysis of the measured equation of invariance”. *IEEE Transactions on Antennas and Propagations*, 43:1168–1171, October 1995.
- [24] J.R. Mosig. Arbitrarily shaped microstrip structures and their analysis with a mixed potential integral equation. *IEEE Transactions on Microwave and Theory*, 36:314–323, February 1988.
- [25] B.D. Popovic and D.N. Filipovic. Theory of power frequency proximity effect for strip conductors. *Proceedings of Institution of Electrical Engineering*, 8:839–842, September 1975.
- [26] A.J. Rainal. Computing inductive noise of chip packages. *ATT Bell Laboratories Technical Journal*, 1:177–195, January 1984.
- [27] O.M. Ramahi, A. Khebir, and R. Mittra. Numerically derived absorbing boundary condition for the solution of open region scattering problems. *IEEE Transactions on Antennas and Propagations*, 39:350–353, March 1991.

- [28] O.M. Ramahi and R. Mittra. Finite element analysis of dielectric scatterers using the absorbing boundary condition. *IEEE Transactions on Microwave Theory and Techniques*, 25:3043–3045, July 1989.
- [29] M.N. Sadiku and L.C. Agba. A simple introduction to the transmission-line modeling. *IEEE Transactions on Circuits and Systems*, 37:991–999, August 1990.
- [30] D.M. Sheen, S.M. Ali, and M.D. abouzahra. Application of the three-dimensional finite-difference time-domain method to the analysis of planar microstrip circuit. *IEEE Transactions on Microwave Theory and Techniques*, 38:849–857, July 1990.
- [31] P. Silvester. TEM wave properties of microstrip transmission lines. *Proceedings of Institution of Electrical Engineer*, 115:43–48, January 1968.
- [32] P. Silvester and M.S. Hsieh. Finite element solution of 2-dimensional exterior-field problems. *Proceedings of Institution of Electrical Engineering*, 118:1743–1747, December 1971.
- [33] H.E. Stinehelfer Sr. An accurate calculation of uniform microstrip transmission lines. *IEEE Transactions on Microwave Theory and Techniques*, 16:439–444, July 1968.
- [34] Y. Taguchi, K. Miyauchi, K. Eda, and T. Ishida. A GHz-band ceramic multi-layer substrate and its application to a hybrid IC. *IEEE MTT-S Digest*, pages 1325–1328, June 1993.
- [35] T. Wang, R.F. Harrington, and J. Mautz. The equivalent circuit of a Via. *IEEE Transactions*, 4:97–123, April 1987.

- [36] T. Wang, R.F. Harrington, and J. Mautz. Quasi-static analysis of a microstrip Via through a hole in ground plane. *IEEE Transactions on Microwave Theory and Techniques*, 36:97–123, June 1988.
- [37] W.T. Week, L.L. Wu, M.F. McAllister, and A. Singh. Resistive and inductive skin effect in rectangular conductors. *IBM Journal of Research and Development*, 23:652–660, November 1979.
- [38] N. Yoshida and I. Fukai. Transient analysis of a stripline having a corner in three-dimensional space. *IEEE Transactions on Microwave Theory and Techniques*, 34:491–498, May 1984.
- [39] X. Zhang, J. Fang, K.K. Mei, and Y. Liu. Calculation of the dispersive characteristics of microstrip by the time domain finite difference method. *IEEE Transactions on Microwave Theory and Techniques*, 36:263–267, February 1988.
- [40] S.S. Zivanovic, K.S. Yee, and K.K. Mei. A subgridding method for the time-domain finite-difference method to solve maxwell’s equation. *IEEE Transactions on Microwave Theory and Techniques*, 3:471–479, March 1991.

Appendices

Appendix A: Acronyms

| | |
|-------|---|
| IC | Integrated Circuit |
| MCM | Multi-Chip Module |
| VLSI | Very Large Scale Integrated circuit |
| CAD | Computer-Aided Design |
| TEM | Transverse Electro Magnetic |
| VFEM | Vector Finite Element Method |
| MEI | Measured Equation of Invariance |
| GHz | GigaHertz |
| FD-TD | Finite-Difference Time-Domain |
| TLM | Transmission Line Matrix |
| MDS | Microwave Design System |
| SIG | Silicon Graphic Incorporated |
| HTMEI | Hybrid edge/nodal FEM with the Three-Component MEI Boundary Condition |

Appendix B: Flow Chart of the Computer Program

The block diagram of the computer code is shown in Figure B.1. The function for each block is explained below:

- The structure parameters for the transmission line — The structure parameters are stored in data files that contain the dimensions of the transmission line structure and the characteristics of the materials used in the transmission line.
- Construct the matrix equation of vector Helmholtz's equation by using the hybrid edge/nodal FEM — From the structure parameters of the transmission line, we calculated the relations between any two elements in a small triangular cell, then constructed the matrix equation by assembling all the small triangular cells. The formulae are described in Section 5.1.
- Sinusoidal-shape metrons — We used sinusoidal-shape metrons for the components of Fourier series which are used to approximate the current and charge distributions on the surface of the conductor. The theory is described in Section 4.3.2.
- Calculate the 3-component MEI cells for the boundary condition — From the metrons we calculate the 3-component MEI cells, which are linear equations for the relation of the boundary element and its neighboring elements. The theory, and formulae are described in Chapter 4.
- Apply 3-component MEI boundary condition on the outer elements of the matrix equation — We applied the 3-component MEI boundary condition on the boundary elements of the numerical mesh, which is constructed by assembling

all the small triangular cells, by replacing the MEI boundary equations for the rows of boundary element in the matrix equation. Section 5.2 and 5.3 describe the theory in more detail.

- HTMEI matrix equation — We call the matrix equation with 3-component MEI boundary condition the HTMEI matrix equation, which is defined in Section 5.3.
- Solve the eigenvalues of HTMEI matrix equation — By rearranging the HTMEI matrix equation, we form an eigenvalue equation. The eigenvalue of the HTMEI matrix equation is the square of the complex propagation constant. The real part of the complex propagation constant is related to attenuation constant of the transmission line by Equation (3.9). The formulae and calculations are described in Section 3.2.2.
- Transmission loss of the transmission line — The eigenvalues of the HTMEI matrix equation are squares of the propagation constants of the various modes. The real part of the complex propagation constant is the attenuation constant. The transmission loss of the transmission can be calculated from the attenuation constant by using Equation (3.9).
- The electric field distribution on the cross section of the transmission line — The eigenvector of the HTMEI matrix equation is the magnitude of electric field intensity on the elements of the matrix equation. The electric field distribution on the cross section of the transmission line is described by the electric field intensity on the elements.

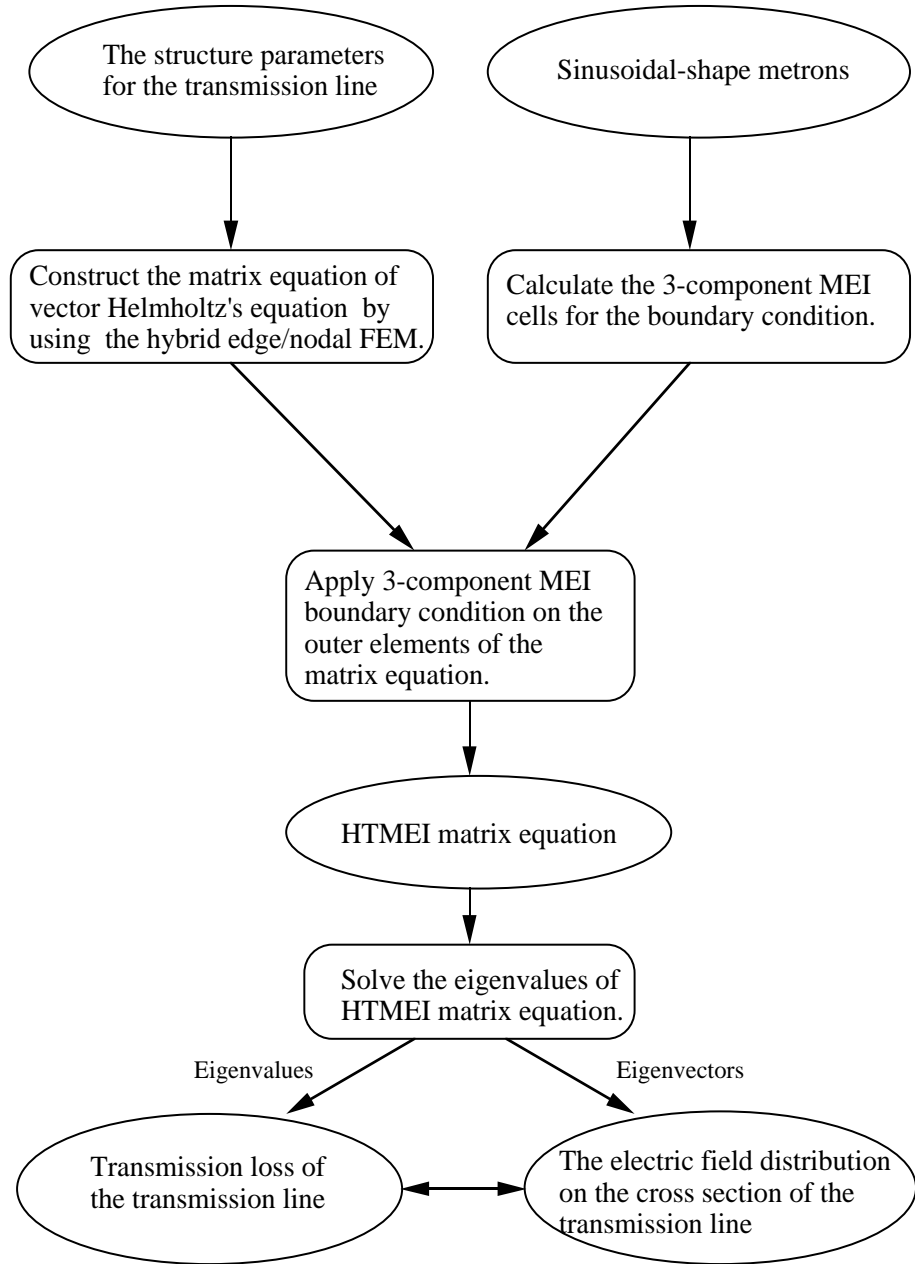


Figure B.1: The flow chart of the computer code

Appendix C: Main Program of the Field Calculation

```

C*****
C Main program for "The field calculation by using the hybrid
C edge/nodal VFEM with 3-component MEI boundary condition"
C*****
C***** Field Distribution on the cross section of a*****
C***** Microstrip. (Using Hankel Function as *****
C***** its Green's Function) *****
C***** *****
C***** Apply the Mei mesh and replace FE mesh *****
C***** both in XYZ directions. *****
C***** *****
C*****
C
C Unit number assignment for input/output data:
C 1 (INPUT) = Fortran Input File number for Z-Mei Cells
C 11 (INPUT) = Fortran Input File number for XY-Mei Cells
C 2 (INPUT) = Fortran Input File number for Edges on Elements
C 3 (Input) = Fortran Input File number for Nodes on Elements
C 13 (Input) = Fortran Input File number for mu on Elements
C 23 (Input) = Fortran Input File number for epsilon on Elements
C 4 (INPUT) = Fortran Input File number for node Location
C 14 (INPUT) = Fortran Input File number for 2 end points of Edge
C 5 (INPUT) = Fortran Input File number for Structure Geometry
C 15 (INPUT) = Fortran Input File number for existed Eigenvalue Ga
C 6 (OUTPT) = Fortran Outut File number for simulation result
C 7 (OUTPT) = Fortran Outut File number for Structure echo
C 71 (OUTPT) = Fortran Outut File number for Matlab Plot
C 72 (OUTPT) = Fortran Outut File number for Matlab Plot
C IERR = Error Flag, zero if all is well
C
C Definition for the constant in the program:
C Nodes = Number of Nodes Used in Problem
C Lines = Number of Lines Used in Problem
C Nelmts = Number of Element in Model for grid nodes
C Nelmt2s = Number of Element in Model for lines
C Nmeis = Number of Z-Mei Cell in Model
C Nmei2s = Number of XY-Mei Cell in Model
C X, Y = Nodal Coordinates
C Xedge, Yedge = Edge Coordinate
C ceps = The permitivity of elements
C urs = The permeability of elements
C Potent = Nodal and Line Potential Array
C NVTX = List of Nodes for Each Element
C NETX = List of Lines for Each Element
C NVMEI = List of Nodes for Each Z-MEI cell
C NVMEI2 = List of Edges for Each XY-MEI cell
C Cphi = The 6 E-field on edges due to 6 metrones
C Cmei = The MEI solution for each MEI node(edge)
C
C=====
C GLOBAL DECLARATION -- SAME IN ALL PROGRAM SEGMENT
C=====
Parameter(maxnod=509,maxlin=1412,maxelm=928,maxmei=128)
complex cpotent, cs, mts, cphi, cmei, ceps

```

```

complex tel,sel
common /params/ ierr,nxy
common /problm/ nodes, nelmts, nmeis, ncons, x(maxnod), y(maxnod),
1      xedge(maxlin),yedge(maxlin),lines,nelmt2s,
1      ceps(maxelm),nmei2s, nvmei2(8,maxmei),
1      urs(maxelm), iedge1(maxlin), iedge2(maxlin),
2      nvtx(3,maxelm), nvmei(8,maxmei), netx(3,maxelm)
common /matrix/ cs(maxnod+maxlin,maxnod+maxlin),
1      mts(maxlin,maxlin)
common /workng/ sel(3,3), tel(3,3), intg(8),
1      cphi(8,maxnod), cmei(8,maxmei),
2      cphi2(8,maxlin), cmei2(8,maxmei)
C=====
real wr(maxlin),wi(maxlin)
complex lambda,bx(maxlin,maxlin),exy(maxlin)
complex tp2(maxnod,maxnod), tp3(maxnod,maxlin)
c
C
C      Identify and open input/output files
open(unit=1,iostat=inrr,file='meifile',status='old',
1  access='sequential',form='formatted')
open(unit=11,iostat=inrr,file='mei2file',status='old',
1  access='sequential',form='formatted')
open(unit=21,iostat=inrr,file='pecnfile',status='old',
1  access='sequential',form='formatted')
open(unit=2,iostat=inrr,file='elem2file',status='old',
1  access='sequential',form='formatted')
open(unit=13,iostat=inrr,file='ufile',status='old',
1  access='sequential',form='formatted')
open(unit=23,iostat=inrr,file='epsfile',status='old',
1  access='sequential',form='formatted')
open(unit=3,iostat=inrr,file='elemfile',status='old',
1  access='sequential',form='formatted')
open(unit=4,iostat=inrr,file='nodefile',status='old',
1  access='sequential',form='formatted')
open(unit=14,iostat=inrr,file='edgefile',status='old',
1  access='sequential',form='formatted')
open(unit=5,iostat=inrr,file='input',status='old',
1  access='sequential',form='formatted')
open(unit=15,iostat=inrr,file='inputeigen',status='old',
1  access='sequential',form='formatted')
open(unit=6,iostat=inrr,file='output',status='unknown',
1  access='sequential',form='formatted')
open(unit=7,iostat=inrr,file='echo',status='unknown',
1  access='sequential',form='formatted')
open(unit=71,iostat=inrr,file='exy.m',status='unknown',
1  access='sequential',form='formatted')
open(unit=72,iostat=inrr,file='exy2.m',status='unknown',
1  access='sequential',form='formatted')
read(5,119) h,t,h12,w,rf
119 format(e10.4,/e10.4,/e10.4,/e10.4,/e10.4)
read(5,129) er,ur,rcu
129 format(f6.1,/f6.1,/e10.4)

```



```

write(7,208) h,t,h12,w,rf,er,ur,rcu
208 format(/1x,'    Check if the input data are correct:')
!      /1x,10x,'h=',e11.4,3x,'t=',e11.4,'h12=',e11.4,
!      /1x,10x,'w=',e11.4,3x,'f=',e11.4,
!      /1x,10x,'er=',e11.4,3x,'ur=',e11.4,
!      /1x,10x,'rcu=',e11.4)
C
C----- Input the structure dimensions -----
C
C      f=(1e9)*2
C      RK is the wavenumber in air
C
C      er=7.55
C      RK=20.944*2.0
C-----
C      Fetch Data for the edges, nodes location and material
C      properties
C-----
C      call meshin(RK,lambda,er)
C-----
C      Initial the Matrix Equation before calculation
C-----
C      call matinit(nodes+lines,nodes+lines,lines)
C
C*****
C      Assemble Global Matrix Cell by Cell
C-----
C*****
C      do 40 i=1,nelmt2s
C         ie=i
C
C-----
C      Constructs Element Matrices in part I of [Ktt]
C      (Equation 3.15)
C-----
C      call ktt1atr(ie,RK)
C
C-----
C      Embed part I of [Ktt] into Global Matrix CS
C-----
C      call ktt1bd(ie)
C 40 continue
C
C      do 42 i=1,nelmt2s
C         ie=i
C
C-----
C      Constructs Element Matrices in part II of [Ktt]
C      (Equation 3.15)
C-----
C      call ktt2atr(ie,RK)
C
C-----
C      Embed part II of [Ktt] into Global Matrix CS
C-----
C      call ktt2bd(ie)
C 42 continue
C
C      do 44 i=1,nelmts
C         ie=i
C
C-----
C      Constructs Element Matrices in [Ktz] (Equation 3.16)

```

```

C-----
C      call ktzatr(ie,RK)
C-----
C      Embed [Ktz] into Global Matrix CS
C-----
C      call ktzbd(ie)
C 44 continue
C      do 46 i=1,nelmts
C         ie=i
C-----
C      Constructs Element Matrices in [Kzz] (Equation 3.17)
C-----
C      call kzzatr(ie,RK)
C-----
C      Embed [Kzz] into Global Matrix CS
C-----
C      call kzzbd(ie)
C 46 continue
C      do 48 i=1,nelmt2s
C         Construct Elements S and T matrix
C         ie=i
C-----
C      Constructs Element Matrices in [Mtt] (Equation 3.13)
C-----
C      call mttatr(ie,RK)
C-----
C      Embed [Mtt] into Global Matrix CS
C-----
C      call mttbd(ie)
C 48 continue
C*****
C      End of Assembling Global Matrix Cell by Cell
C*****
C-----
C      Apply the Mei Boundary on the node elements
C-----
C      call metrone(RK,er,w,t,h,h12,kiter)
C-----
C      Apply the MEI Boundary to the edge elements
C-----
C      call metroneedge(RK,er,w,t,h,h12,kiter)
C-----
C      From the eigenvalue matrix equation with
C      3-component MEI boundary condition
C-----
C      call Form(bx,tp2,tp3)
C-----
C      Solve the Eigenvalue and Eigenvector by using
C      QR decomposition
C-----
C      call eigen(wr,wi,lambda,bx,exy,tp2,tp3)
C

```

```

C-----
C   Output the eigenvalu and eigenvector of the
C   Lowest propagation mode
C-----
      do 205 i=1,lines
        write(6,207) i,wr(i),wi(i),sqrt(cmplx(wr(i),wi(i)))
207   format('eigenvalue(',i4,')=',e11.4,2x,e11.4,4x,
!   'gamma= ',e11.4,2x,e11.4)
205   continue
        write(7,208) h,t,h12,w,rf,er,ur,rcu
        stop
      end

```